nature nanotechnology

Supplementary information

https://doi.org/10.1038/s41565-024-01791-2

Controlled single-electron transfer enables time-resolved excited-state spectroscopy of individual molecules

In the format provided by the authors and unedited

Table of contents

1. Assignment of the transitions in the spectra of pentacene

The features in the pentacene spectra shown in Fig. 3 and 4 were assigned to transitions as indicated in panels g of these figures. In general, the assignment was guided by considering which transition pathways sequentially open with increasing or decreasing voltage, as well as by the dependence of the population on t_{sweep}. In case of the experiment, in which the molecule is initiated in D_0^+ (Fig. 3), the first two transitions that open with increasing V_{sweep} are the transitions $D_0^+ \rightarrow S_0$ and $D_0^+ \rightarrow T_1$ (see main text), at the threshold voltages (1) and (2), respectively. Note that more than 80% of the population between (2) and (3) was read-out in the D_0^+ state, indicating that most of the population ended up in the T_1 state. This larger rate of tunneling into the T_1 state than into the S_0 state can be explained by a difference in tunneling barrier (see section 2), multiplicity, spin-state overlap and the (position dependent) different spatial overlap between the tip and LUMO and HOMO, respectively. The difference in multiplicity and spin-state overlap gives rise to a ratio of tunneling between $D_0^+ \rightarrow T_1$ and $D_0^+ \rightarrow S_0$ of 3 to 2.

Subsequently, our analysis suggests that at (3) in Fig. 3 two new transitions could potentially become accessible. One of them is the $D_0^+ \rightarrow S_1$ transition. S_1 will immediately decay to the singlet ground state S_0 (see schematic 3A). Since this decay is within one multiplicity and therefore spin allowed, it can safely be assumed to be instantaneous on the time scale of the experiment. The opening of the $D_0^+ \rightarrow S_1 \rightarrow S_0$ pathway will reduce the population in T_1, since it competes with the $D_0^+ \rightarrow T_1$ pathway, also starting at D_0^+ (see Figs. 3g and S1). The ratio of these two pathways is governed by the difference in tunneling barrier, multiplicity and spin-state overlap. The multiplicity and spin-state overlap give a 1 to 3 ratio for the rates of $D_0^+ \rightarrow S_1$ and $D_0^+ \rightarrow T_1$ (note that this is different from the 2 to 3 ratio for $D_0^+ \rightarrow S_0$ and $D_0^+ \rightarrow T_1$, due to the different spatial overlap of wavefunctions). The other new pathway that could open starts with the $T_1 \rightarrow D_0^-$ transition, which is then followed by a $D_0^- \rightarrow S_0$ transition, effectively quenching the T_1 population, see schematic 3B. As clarified further below, with the help of an additional experiment, the results of which are shown in Fig. 4, we recognized that both of these processes contribute to the features observed at (3). Similarly, the feature observed at (6) at a higher sweep voltage could either stem from accessing a transition from D_0^+ to a short lived excited neutral state, or accessing a transition from T_1 to an excited negative charge state. We find from the experiment shown in Fig. 4 that the feature at (6) relates to accessing a $T_1 \rightarrow D_1^-$ transition. At V_{sweep} = 3.2 V we observe another feature, indicating that a transition opens or closes. We tentatively assign the feature to a $D_0^+ \rightarrow T_1 \rightarrow Q_1^-$ pathway, where Q_1^- is a negatively charged quadruplet state with presumably one electron in the HOMO, one in the LUMO and one in a higher-lying orbital, such as the LUMO+1. As indicated in the main text, we refer throughout this work to the orbital electronic levels according to the neutral molecule's states. In contrast to D_0^-, Q_1^- cannot directly decay into the S_0 state, as this would require the simultaneous tunneling of multiple electrons. Since this latter assignment is tentative and Q_1^- is not considered any further, we did not include this transition in the rate equations (section 7).

There are two additional very small steps at (4) and (5) visible in Fig. 3a for the longer durations of the sweep pulse. These features appear at a V_{sweep} relatively close to the D_0^--S_0 charge-degeneracy point at 1.42 V, suggesting that these features might relate to transitions between

states with neutral and negative charge. As will become clear in the following, the visibility of such charge transitions in the signal is low, when read out at the charge degeneracy of a different pair of charge states (for this case at the neutral-positive charge degeneracy). Instead, the visibility is large, if transitions between two charge states are read out at the charge degeneracy corresponding to these two states (for this case at the neutral-negative charge degeneracy). Therefore, we repeated the experiments with a different read-out voltage, mapping the states onto the D_0^- and S_0 states instead of the D_0^+ and S_0 states. The resulting spectra shown in Fig. 3d exhibit very pronounced steps at (4) and (5). To understand these, it is easiest to analyze this spectrum starting at large positive voltages (from right to left). At the right end of the spectrum, V_{sweep} is far beyond the negative-neutral charge degeneracy point at 1.42 V such that every state decays to D_0^- at long t_{sweep}, resulting in a read-out fraction in D_0^- of 1 (Fig. 3d). We recall that the molecule is still initialized in D_0^+, such that for large V_{sweep} it may cascade via the neutral S_0 and T_1 towards D_0^-. However, at a V_{sweep} below (5) but above (4), the cascade via S_0 becomes blocked, since S_0 will not decay into D_0^-, explaining the decrease in the read-out fraction (in D_0^-) in the direction of decreasing V_{sweep} at (5) in Fig. 3d. Decreasing V_{sweep} further to below (4), D_0^- (after its population from T_1) can decay into S_0 such that all the population can transfer into S_0, explaining the additional decrease in the read-out in D_0^- in the direction of decreasing V_{sweep} at (4).

As mentioned above, the transitions assigned to (4) and (5) are also those that cause the small steps at the voltages associated to (4) and (5) in Fig. 3a. However, in Fig. 3a the population in the D_0^- state at the end of the sweep pulse is read-out at the positive-neutral charge degeneracy, causing only a small fraction of D_0^- to be read-out as D_0^+. Analogously, at the left end of the spectrum in Fig. 3d, transitions between states with positive and neutral charge are read out at the negative-neutral charge degeneracy, explaining the reduction in read-out signal from Figs. 3a to d below the voltage of feature (1). In both cases, the magnitude of the read-out signal depends on the rates of the competing pathways that are indicated by the thickness of the arrows in the read-out diagrams in Figs. 3c and f.

There are two approaches to further substantiate the above interpretation of the data shown in Fig. 3. First, data can be taken at different lateral tip positions above the molecule, see section 3. Second, as indicated in the main text, we can adapt the set pulse to initialize the population in the neutral state, with a preselected ratio in S_0 and in T_1 (for pentacene we choose to approximately equally populate S_0 and T_1, see methods). This different starting configuration modifies the weight of the different pathways and eliminates pathways that start at D_0^+ and thereby can aid the assignment of spectral features to specific electronic transitions. The results are shown in Figs. 4a and d. In Fig. 4a around $V_{sweep} = 0$ V, the initialized population in the T_1 state will stay in T_1 during the sweep pulse (except for the slow direct decay into S_0) and will be detected as D_0^+ during the read-out. Upon increasing V_{sweep}, two downward steps are observed for the shortest t_{sweep}, at (3B) and (6). At the same V_{sweep} are steps in Fig. 3a. Since processes that start at D_0^+ are excluded in Fig. 4, the observation of these steps in Fig. 4a indicates that the T_1 state is involved, supporting the assignment of $T_1 \rightarrow D_0^-$ to (3B) and $T_1 \rightarrow D_1^-$ to (6). Note, however, that the relative step sizes at (3) are quite different for Figs. 3a and 4a (for the shortest t_{sweep} the signal drops by roughly 2/5 and 1/4 of its preceding value,

respectively). This indicates that the step in Fig. 3a cannot stem from $T_1 \rightarrow D_0^-$ alone but must contain another contribution (which we assigned to $D_0^+ \rightarrow S_1$ (3A)), not contributing in Fig. 4a.

For small enough V_{sweep}, T_1 can decay into D_0^+ (8). This experiment also allows accessing the $S_0 \rightarrow D_0^+$ transition (7) at voltages more negative than the positive-neutral charging hysteresis at around -2.8 V. This transition is not accessible, when initializing the molecule in D_0^+.

The initial preparation of the molecule in the neutral state further allows us to vary the initial population of the triplet state by slightly modifying the set pulse sequence. The results of this additional parameter variation are shown in Fig. S3 and confirm that all the transitions that were assigned to start with the triplet state indeed scale with the initial triplet population (see section 4).

2. Barrier height

Fig. S1 shows the effect of the tunneling-barrier height on the rates of tunneling between tip and molecule. The single-particle pictures, shown in Fig. S1b and d, indicate a smaller tunneling barrier for tunneling in or out of the LUMO (purple area) than for tunneling in or out of the HOMO (purple plus light blue area). Based on this barrier-height argument, we qualitatively drew the arrows in the many-body diagrams with different relative thicknesses throughout this work. For the tip side of the tunneling barrier, the following rule applies: for electron tunneling processes from the tip to the molecule (that is, when the molecule gets charged more negative, e.g. $D_0^+ \rightarrow S_0$, $S_0 \rightarrow D_0^-$), the tunneling barrier is the smallest for (energetically allowed) processes with a final state having the highest energy (see Fig. S1a, b), whereas upon tunneling an electron from the molecule to the tip (that is, when the molecule gets charged more positive, e.g. $D_0^- \rightarrow S_0$, $S_0 \rightarrow D_0^+$), the barrier is the smallest for processes with the final state having the lowest energy in the many-body energy diagram (see Fig. S1c, d). Note that, the simple rule stated above applies only to tunneling through a vacuum barrier[1], as considered here.

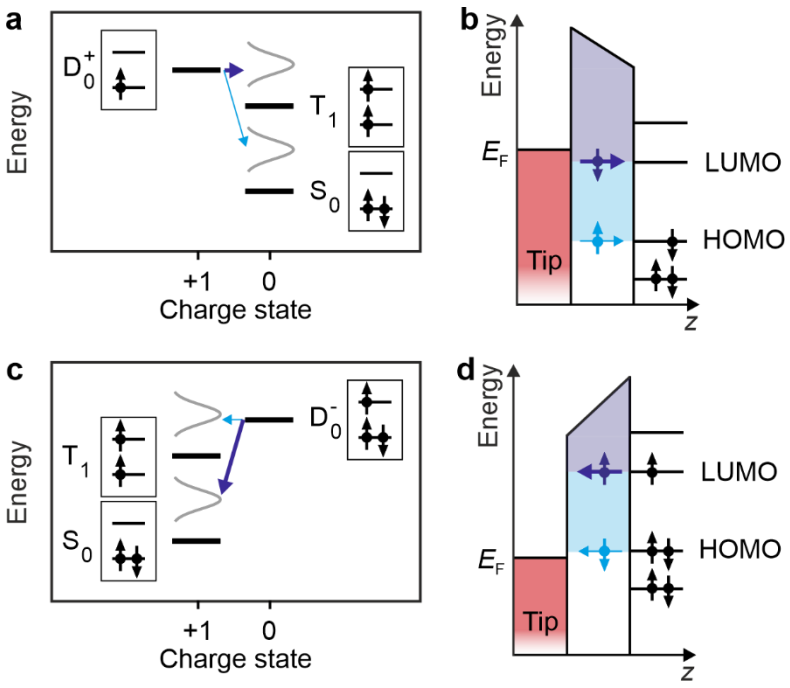

Figure S1 | Qualitatively inferring the barrier heights and tunneling rates from connecting to the single-particle picture. a, **c**, Many-body energy diagrams for an exemplary sweep voltage and a read-out voltage. Two transitions are highlighted in light and dark blue, with their relative rates indicated qualitatively by the thickness of the arrows. **b**, **d**, Single-particle pictures showing the tunneling barrier for the processes indicated in **a**, **c**, respectively. The vacuum-tunneling barriers are indicated by the colored areas. From the single-particle pictures it is apparent that tunneling in or out of the LUMO has a lower tunneling barrier than tunneling in or out of the HOMO.

3. Varying the lateral tip position

To further scrutinize the interpretation of the data shown in Figs. 3a and d, we performed experiments at three different lateral tip-positions above the molecule. The results for three t_{sweep} are displayed in Figs. S2a, b and c. The spectra were taken at the positions indicated in the AC-STM images[2] of the HOMO and LUMO densities shown in Figs. S2f and g. These images show that upon moving at constant height from position I to III, the tunneling rates to the HOMO and LUMO are both reduced. This explains the increase of the fraction in D_0^+ during the read-out in Fig. S2a from position I to III between voltages associated to (1) and (2) and above (3): with a decreasing tunneling probability from position I to III, a larger fraction remains in the initialized D_0^+ state. However, the fraction that is read-out between voltages corresponding to (2) and (3) seems much less affected by the lateral tip position, as can be seen in Figs. S2b and c. This supports our assignment that the plateau between voltages of (2) and (3) is governed by two competing tunneling rates, namely those corresponding to the $D_0^+ \rightarrow S_0$ and the $D_0^+ \rightarrow T_1$ transitions. As this fraction is – within error margins – the same for the long t_{sweep} used in Fig. S2c, it can be concluded that these competing transitions are both suppressed to a similar extent by changing the tip position from I to III.

Fig. S2b shows two additional peaks in the data: one just below the voltage corresponding to (3) and another between the voltages corresponding to (5) and (6). A similar peak is observed in the data measured on PTCDA (at (9) in Fig. 5a). We assign it to accessing an excited triplet state, which will be explained in section 5. As the first small peak in Fig. S2b is located in proximity to the V_{sweep} where the $D_0^+ \rightarrow S_1$ transition becomes accessible (3), it is assigned to a transition to T_2, because of the experimental evidence that a higher-lying triplet state lies close to the S_1 state of pentacene[3,4]. The reasoning why this leads to a peak in the data is analogous to the observed peak at (9) for PTCDA (Fig. 5a and section 5). We note that the $D_0^+ \rightarrow T_2$ transition assigned to the step at (9) might (partially) also proceed via S_1 followed by intersystem crossing to T_2, hence as $D_0^+ \rightarrow S_1 \rightarrow T_2$. The likelihood of such an intersystem crossing pathway competing with a direct decay of S_1 to S_0 was found to be strongly dependent on the exact energy level alignment of S_1 and T_2, which depends on the environment[3,4].

The feature in Fig. S2b at 1.7 V we assign to accessing a transition to a higher-lying triplet excited state, here called T_3, at which one electron occupies the HOMO and another a higher-lying unoccupied orbital. Interestingly, these peaks only show up at spatial positions laterally displaced from the HOMO and LUMO density maxima, indicating that higher-lying orbitals with a different spatial distribution are involved, which is consistent with the assignment as a transition to a higher-lying excited triplet state (see section 5).

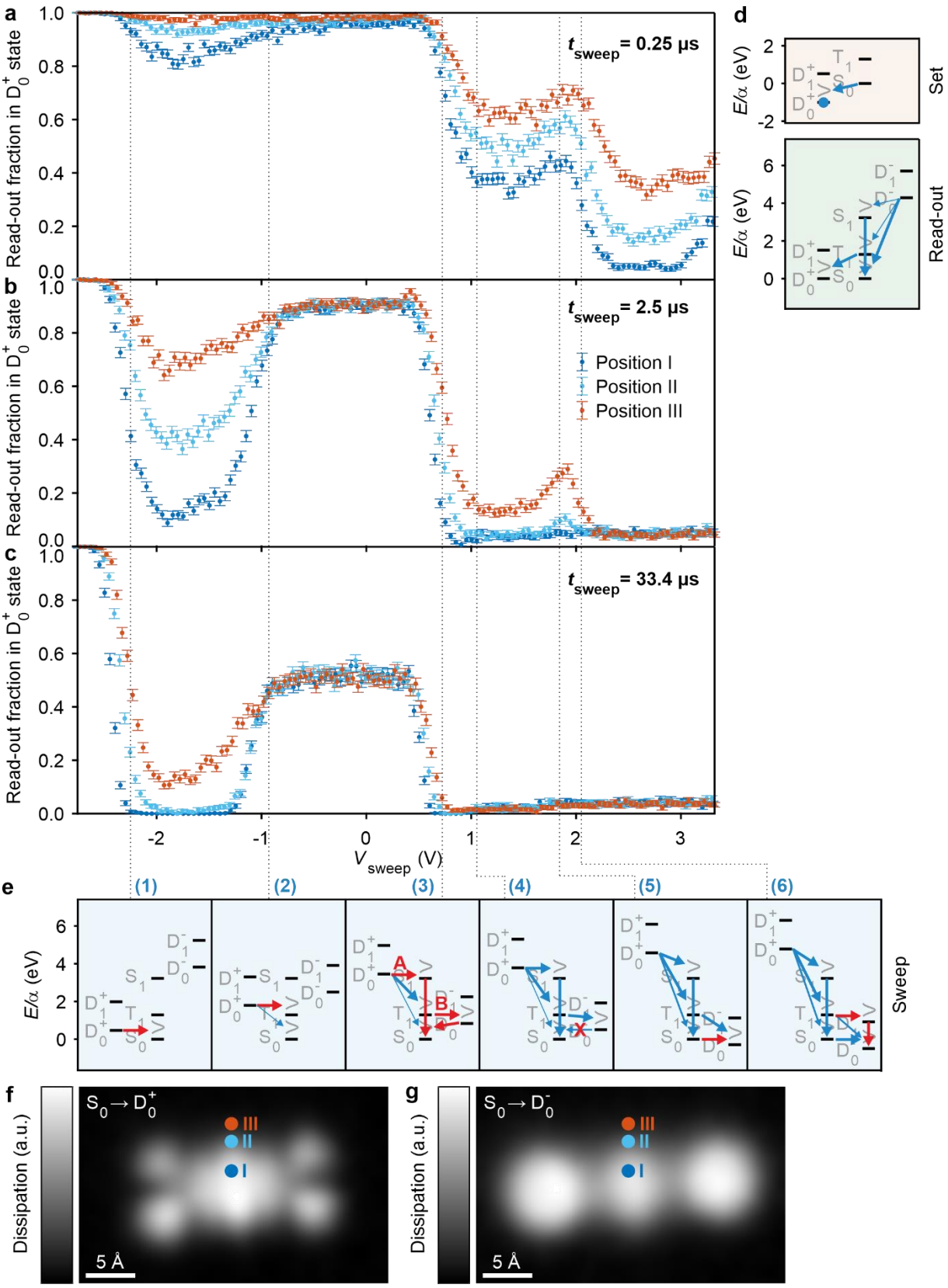

Figure S2 | Excited-state spectroscopy of pentacene at different lateral tip positions. a-c, Measured read-out fraction in the D_0^+ state versus the applied gate voltage during the sweep pulse V_{sweep}, for three different tip positions and for three different sweep pulse durations. The measurements were performed above the same individual molecule as in Figs. 3 and 4 with a voltage pulse sequence similar to Fig. 2a, using a set pulse to initialize the molecule in D_0^+ (V_{set} = -3.8 V) and read-out at the S_0-D_0^+ degeneracy

($V_{\text{read-out}}$ = -2.8 V). Each data point corresponds to the normalized discrete counts of 640 pump–probe cycles and the error bars are ± s.d.; see Methods. **d**, Many-body energy diagrams of the transitions taking place during the set pulse and at the beginning of the read-out phase for the spectra shown in **a**-**c**. **e**, Many-body energy diagrams of the transitions taking place at the sweep voltages indicated by the dotted lines. The arrows, crosses and dots are analogous to Fig. 3g. Panel **b** shows two additional features at 0.4 and 1.7 V, respectively, which are not indicated in **e** but described in the text. **f**, **g**, AC-STM images[2] of the same pentacene as in **a**-**c** indicating the three positions where the spectra shown in **a**-**c** were measured (oscillation amplitude A = 1 Å): $S_0 \rightarrow D_0^+$ (HOMO): Δz = -2.6 Å, V_G = -2.9 V, $V_{\text{a.c.}}$ = 1.2 V peak-to-peak (V_{pp}), and $S_0 \rightarrow D_0^-$ (LUMO): Δz = -2.0 Å, V_G = 1.43 V, $V_{\text{a.c.}}$ = 1.2 V_{pp}). Δz is given with respect to the setpoint Δf = -1.443 Hz at V = 0 V, A = 3 Å. Note that images **f** and **g** were taken at a tip-sample distance 2.6 and 2.0 Å smaller than used for the excited-state spectroscopy **a**-**c**, respectively. Therefore, in the spectra in **a**-**c** the dependence of tunneling rates on the lateral position is less pronounced than in the AC-STM images.

4. Controlling the initial populations

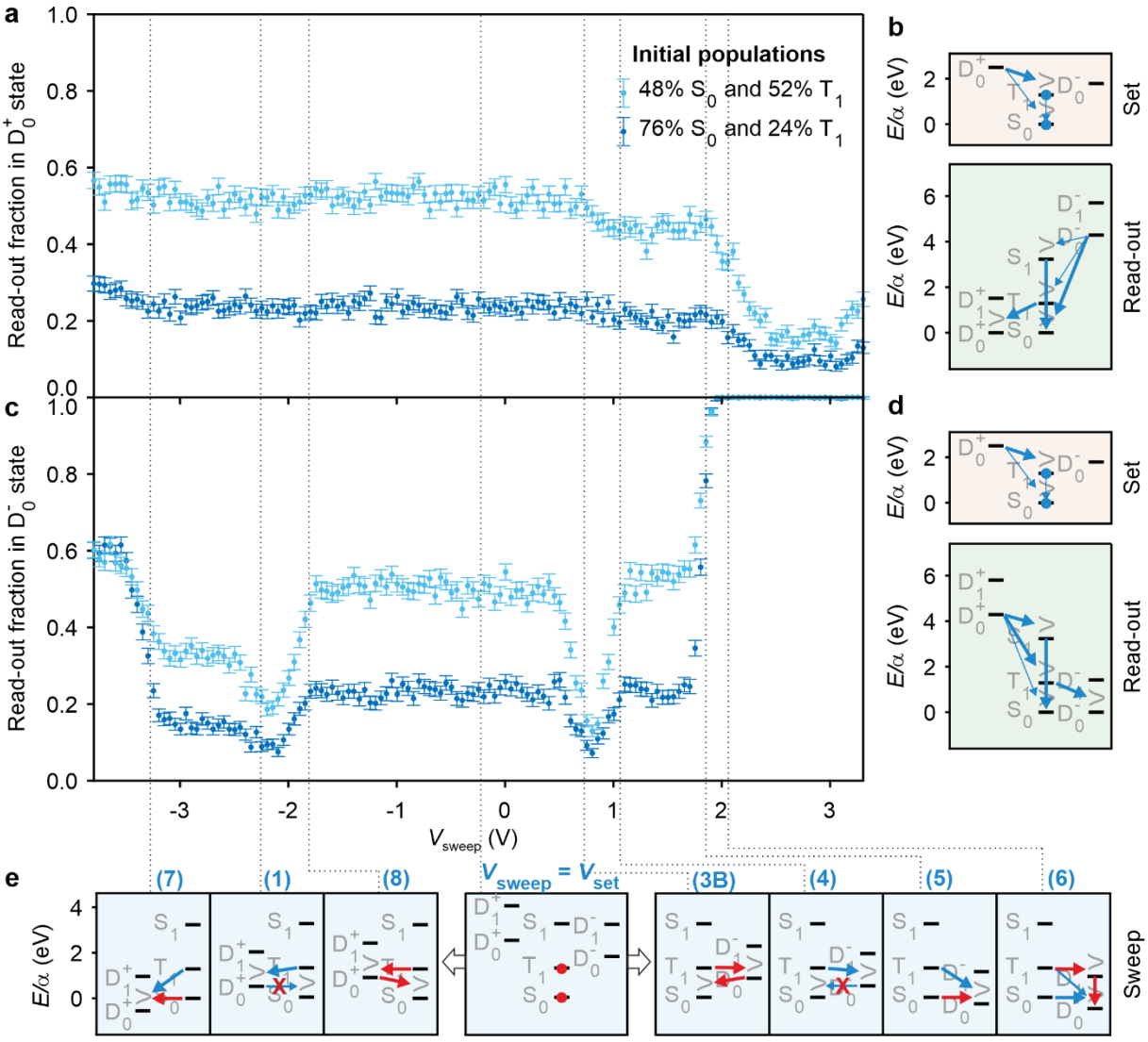

Figure S3 | Excited-state spectroscopy of pentacene, initialized in the neutral charge state with different S_0 and T_1 populations. a, **c**, Plot of the measured read-out fraction in the D_0^+ and D_0^- states, respectively, versus V_{sweep}. Measurements were performed with a voltage pulse sequence similar to Fig. 2a. Two different set pulse sequences were used to initialize the molecule with different initial populations in S_0 and T_1, as indicated (see for more details the Methods section). The read-out was at the S_0-D_0^+ ($V_{read\text{-}out}$ = -2.795 V) and S_0-D_0^- ($V_{read\text{-}out}$ = 1.416 V) degeneracy for **a** and **c**, respectively. A t_{sweep} of 0.14 µs for **a** and 2.8 µs for **c** was used. Each data point corresponds to the normalized discrete counts of 640 pump–probe cycles and the error bars are ± s.d.; see Methods. **b**, **d**, Many-body energy diagrams of the transitions taking place during the set and at the beginning of the read-out phase for the spectra shown in **a** and **c**, respectively. **e**, Many-body energy diagrams of the transitions taking place at the sweep voltages indicated by the dotted lines. The arrows, crosses and dots are analogous to Fig. 3g. Note that if the sweep voltage is close to the set voltage (between (8) and (3B)) the population remains in the T_1 and S_0 state (see diagram at $V_{sweep} = V_{set}$). Only upon reducing or increasing V_{sweep} outside this range different transition channels open and/or close as indicated.

Fig. S3 shows the resulting spectra for initializing the molecule with different populations of the T_1 and S_0 state using different set pulse sequences. This was achieved by varying the duration of the second pulse of the set-pulse sequence, since the T_1 state decays during this

period to the S_0 state according to its molecule-specific lifetime. Fig. S3a shows that the steps at (3B) and (6) scale with the initial T_1 population, lending further support that (3B) and (6) involve the T_1 state. Fig. S3b shows a similar scaling in the voltage region between (7) and (5). This confirms that the T_1 state is also involved in (1), (4) and (8). In contrast, the high and low voltage regions are not affected by the ratio of T_1 and S_0 population at the beginning of the sweep pulse. This confirms the interpretation that at these high and low voltages, all the initial population will end up in a single charge state (D_0^- at (5) and D_0^+ at (7)). Therefore, it is not affected by changing the initial T_1 population.

5. Assignment of the transitions in the spectra of PTCDA

Figure 5 shows the excited-state spectroscopy spectra for PTCDA, with read-out at the S_0-D_0^+ degeneracy. Although the data with a set pulse sequence that brings the molecule to the S_0 or T_1 state (Fig. 5d) has a very similar qualitative appearance as the corresponding pentacene data (Fig. 4a), the data for initializing the molecule in the D_0^+ state (Fig. 5a) shows substantial differences with respect to the corresponding pentacene data (Fig. 3a).

The first difference is that there are two downward steps present at thresholds (3B) and (3A) in Fig. 5a, instead of a single step. From comparing to Fig. 5d where transitions starting at D_0^+ are excluded, the step at (3B) can be assigned as the quenching of T_1 via D_0^-, while the step at (3A) is caused by a transition starting at D_0^+ and is assigned to $D_0^+ \rightarrow S_1$. In other words, the same transitions happen for PTCDA as for pentacene, but in contrast to pentacene, (3A) and (3B) are well separated in voltage for PTCDA.

The second striking difference is that another step is visible at (9). Interestingly, this step is upwards, indicating that the population in D_0^+ is increased. No such step is appreciable in the data for initialization in the neutral states (Fig. 5d), indicating that a transition starting at D_0^+ is involved. The upward step suggests that a long-lived state is accessed. We hypothesize that an excited triplet state T_2 is populated, in which one electron is present in the HOMO and the other in a state higher in energy than the LUMO, that is a higher-lying unoccupied orbital (T_2 may also entail further contributions of other configurations). This state is expected to decay to the T_1 state with a fast decay rate because this transition is spin conserving[5] (see Fig. S4a).

With our spectroscopic method we can test this hypothesis experimentally. To this end, we performed two experiments, similar to those in Figs. 4 and 5d, but once using a set pulse sequence that prepares the molecule in the state under investigation (that we propose to be T_2), and once using a set pulse with a voltage that is just too low to allow a transition into this state. The results are shown in Fig. S4c. Interestingly, upon populating this state, the read-out fraction in the charge state has increased, especially in the voltage ranges where the read-out population directly reflects the T_1 population (below (1) and between (8) and (3B)). The related state seems, thus, to behave identical to the T_1 state, except that it is populated at higher voltages. If instead a long-lived neutral excited state would be populated, which does not decay to T_1 on the timescale of the sweep pulse (a few µs), the resulting signal in Fig. S4c is expected to clearly deviate around the voltage for which the many-body diagram of Fig. S4d is drawn. If the state decayed to T_1, this population would stay in T_1 at this voltage (neglecting the much longer decay time of T_1 to S_0), as shown in Fig. S4d. If the populated state itself was long-lived, the population in this state would decay back to D_0^+ at this voltage, and from there to S_0 (see dotted arrows in Fig. S4d). In other words, the green curve in Fig. S4c would then be even lower than the red curve in a small range above (8), which is not observed in Fig. S4c. We, therefore, assign feature (9) to the population of a higher-lying excited triplet state that immediately decays to the T_1 state.

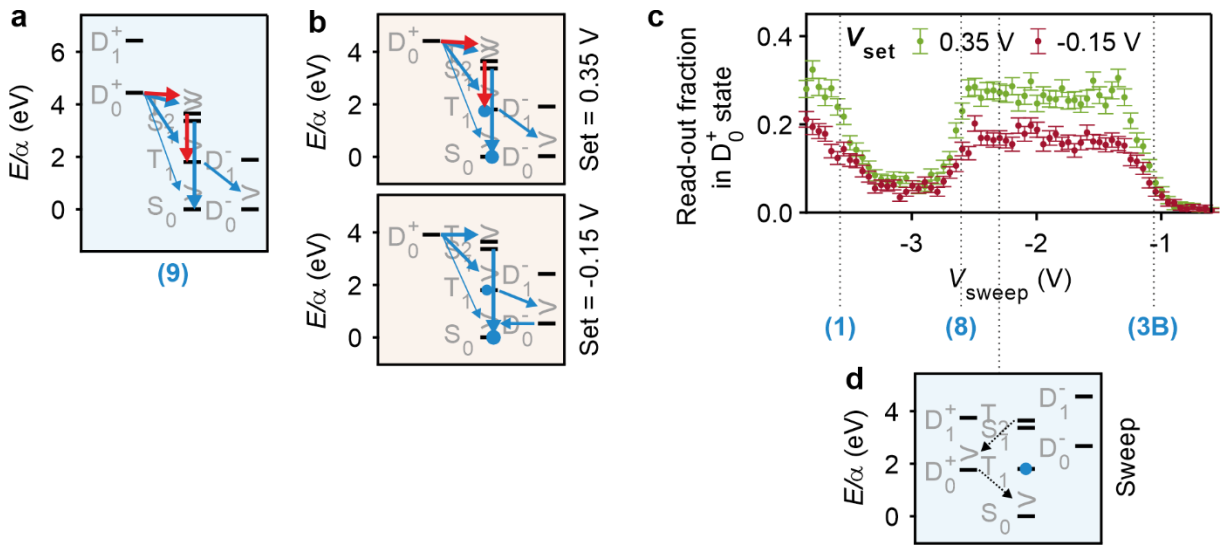

Figure S4 | Excited-state spectroscopy to assess the origin of feature (9). a, Many-body energy diagram of the assumed transition pathway opening at (9). **b**, To experimentally test this hypothesized transition to T_2, excited state spectroscopy was performed with a modified set pulse sequence. The first set pulse initializes the molecule in D_0^-. Two differentvoltages of the second set pulse were used that allow or not allow the proposed $D_0^+ \rightarrow T_2$ transition, as is illustrated by the many-body energy diagrams corresponding to these two voltages. The arrows and dots are analogous to Fig. 3. **c**, Resulting plot of the measured read-out fraction in the D_0^+ state versus V_{sweep} for the two different set voltages used. This data was measured using a duration of the second set pulse t_{set} of 0.74 µs and a sweep pulse duration t_{sweep} of 2.96 µs. Each data point corresponds to the normalized discrete counts of 640 pump–probe cycles and the error bars are ± s.d.; see Methods. **d**, Many-body energy diagram at the voltage indicated by the dotted line in c, showing that if the T_2 population decayed to T_1, it will stay in T_1 at this voltage. In case a part of the population would still be populating T_2 at the end of the set pulse sequence, it would decay via D_0^+ to S_0 at this voltage (dotted arrows), causing a reduction in read-out fraction in D_0^+, which is not observed in **c**.

6. Assessment of the assignment of the transitions

This section critically reviews the assignment of the important transitions as explained in the main text and in the sections 1, 3, 4 and 5 and provides a general strategy, how the different transitions can be assigned, for example, in a future study of other molecules.

As a first step, Kelvin-probe force spectroscopy provides the voltages at which the molecule changes its charge state, corresponding to a transition between the two ground states of different charge. Which charge-state transition is observed can be confirmed by the AC-STM images (see Fig. 3 for pentacene and Fig. 5 for PTCDA), which reflect the orbital densities of the respective molecular orbital being tunneled into or out of. $D_0^+ \rightarrow S_0$ and $S_0 \rightarrow D_0^-$ are associated to tunneling into the HOMO and the LUMO respectively, the densities of which are observed in AC-STM, allowing us to identify the positive-neutral and neutral-negative degeneracies. Transition (1) is the first transition which occurs upon increasing V_{sweep} from the positive-neutral degeneracy and can therefore be assigned to the $D_0^+ \rightarrow S_0$ transition. The assignment of (2) to accessing $D_0^+ \rightarrow T_1$ is confirmed by the fact that the accessed state is long-lived and decays with a triple-exponential decay (see ref. 6 for pentacene and Extended Data Fig. 4 for PTCDA).

Based on this assignment the molecule can be prepared in T_1, and the value of the plateau between (8) and (3B) in Fig. 4 and Fig. 5d reflects the relative T_1 population. The first transitions that will open upon decreasing or increasing V_{sweep} are those to the cationic and anionic ground states, that is, forming D_0^+ or D_0^-, respectively. Thus, (8) and (3B) can be assigned to $T_1 \rightarrow D_0^+$ and $T_1 \rightarrow D_0^-$, respectively. Assuming similar relaxation energies for the different transitions, the S_0-T_1 gap can be derived from $D_0^+ \rightarrow S_0$ and $D_0^+ \rightarrow T_1$. Using this gap and the voltage of the $T_1 \rightarrow D_0^-$ transition, the voltage for accessing the $S_0 \rightarrow D_0^-$ transition (5) can be estimated precisely enough to confirm the assignment of the feature corresponding to (5).

Furthermore, the reorganization energy can be obtained from the difference between the $D_0^+ \rightarrow T_1$ and $T_1 \rightarrow D_0^+$ transition energies. Assuming similar reorganization energies (see section 10), the $S_0 \rightarrow D_0^+$ (7) and $D_0^- \rightarrow S_0$ (4) transition voltages can be estimated from the known $D_0^+ \rightarrow S_0$ and $S_0 \rightarrow D_0^-$ transition voltages, respectively, to assign the respective features.

The energy of the $S_1 \rightarrow S_0$ transition is well known from luminescence experiments and can therefore be assigned from literature values. Preferentially, values from experiments in similar sample setups (environments) should be used, as the energy level alignment depends on the environment of the molecule. The $S_1 \rightarrow S_0$ transition of both pentacene and PTCDA have been measured for a single molecule on a few monolayers of NaCl on a Ag substrate, using a Ag covered tip apex, and we use those values for comparison here: 2.26 eV (ref. 7) and 2.45 eV (ref. 8), respectively. Using an estimate of the lever arm (we typically find values around $\alpha = 0.7$, see section 9), the $D_0^+ \rightarrow S_1$ transition (3A) can be assigned.

This leaves the assignment of the $T_1 \rightarrow D_1^-$ transition (6). For a preparation of the molecule in T_1, the $T_1 \rightarrow D_1^-$ transition is the second transition towards more positive sweep voltage, following the $T_1 \rightarrow D_0^-$ transition, being the first.

7. Rate equations and fitting

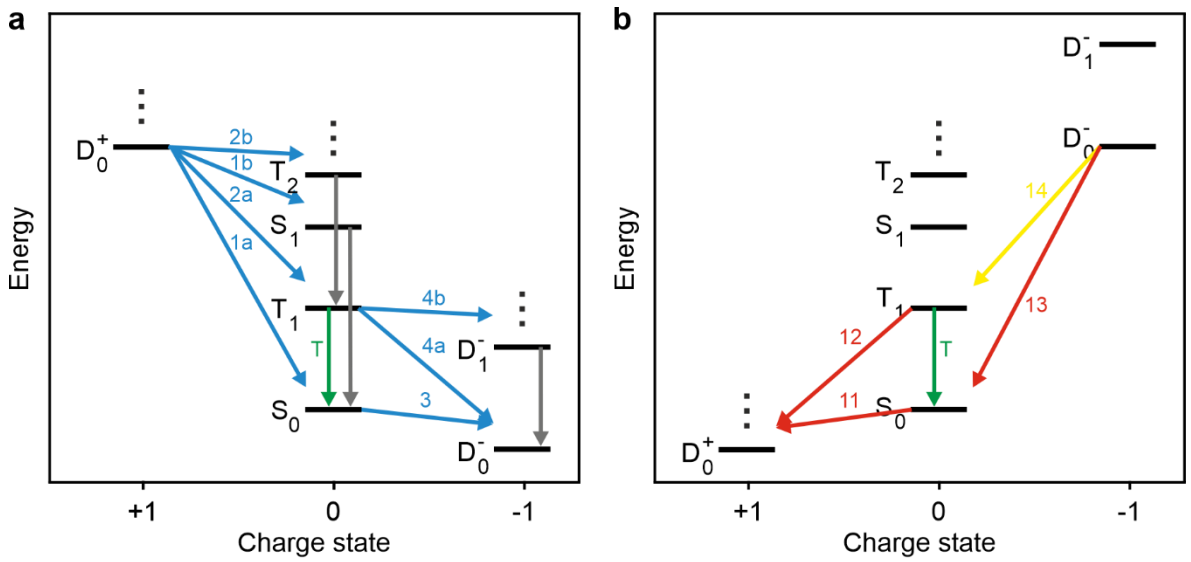

Figure S5 | Definition of the transitions and their rates. Many-body diagrams at the largest positive (**a**) and largest negative (**b**) gate voltage used, indicating the labels of the transitions by numbers attached to the arrows. The corresponding rates are indexed according to these labels. Blue (red) arrows are used to indicate an electron tunneling process from the tip (molecule) to the molecule (tip), while the gray arrows indicate the immediate decay processes from a higher-lying excited state to the lowest state of the same multiplicity and charge. The green arrow indicates the $T_1 \rightarrow S_0$ decay. Transition 14 is indicated in yellow, since this transition is not taken into account in the final rate equations that describe the populations during the sweep pulse, for reasons explained in the text. For similar reasons transitions from D_0^- to S_1 or T_2 during the sweep pulse are also not included.

To fit the data, we describe the time-dependent populations of the different states S_0, T_1, S_1, T_2, D_0^+, D_0^-, and D_1^- during the sweep period by sets of differential equations. In the following, we use the italicized labels of the states to describe their populations. The transition rates between these states are used as visualized in Fig. S5, serving as a definition of the corresponding indices. We assume that the relaxation between states of the same charge and the same multiplicity is fast compared to all other time scales of the experiment. Hence, for the rate equations we assume these relaxations to be immediate. Therefore, a transition into S_1 has the same effect as a transition into S_0, for example. Most rates depend on the applied voltage and the tunneling conditions, as described further below. The resulting set of differential equations reads

$$\frac{\mathrm{d}}{\mathrm{d}t} D_0^+(t) = -(k_{1\mathrm{a}} + k_{1\mathrm{b}} + k_{2\mathrm{a}} + k_{2\mathrm{b}}) D_0^+(t) + k_{12} T_1(t) + k_{11} S_0(t)$$

$$\frac{\mathrm{d}}{\mathrm{d}t} T_1(t) = -(k_{4\mathrm{a}} + k_{4\mathrm{b}} + k_{12} + k_{\mathrm{T}}) T_1(t) + (k_{2\mathrm{a}} + k_{2\mathrm{b}}) D_0^+(t) + k_{14} D_0^-(t)$$

$$\frac{\mathrm{d}}{\mathrm{d}t} S_0(t) = -(k_3 + k_{11}) S_0(t) + (k_{1\mathrm{a}} + k_{1\mathrm{b}}) D_0^+(t) + k_{\mathrm{T}} T_1(t) + k_{13} D_0^-(t)$$

$$\frac{\mathrm{d}}{\mathrm{d}t} D_0^-(t) = -(k_{13} + k_{14}) D_0^-(t) + (k_{4\mathrm{a}} + k_{4\mathrm{b}}) T_1(t) + k_3 S_0(t)$$

For the differential equations, rates k_{1a} and k_{1b} have the same effect. The same holds true for the pair k_{2a} and k_{2b}, as well as the pair k_{4a} and k_{4b}. These pairs are therefore combined to the rates $k_1 = k_{1a} + k_{1b}$, $k_2 = k_{2a} + k_{2b}$ and $k_4 = k_{4a} + k_{4b}$, respectively, leading to the slightly simplified version

$$\frac{\mathrm{d}}{\mathrm{d}t} D_0^+(t) = -(k_1 + k_2) D_0^+(t) + k_{12} T_1(t) + k_{11} S_0(t)$$

$$\frac{\mathrm{d}}{\mathrm{d}t} T_1(t) = -(k_4 + k_{12} + k_\mathrm{T}) T_1(t) + k_2 D_0^+(t) + k_{14} D_0^-(t)$$

$$\frac{\mathrm{d}}{\mathrm{d}t} S_0(t) = -(k_3 + k_{11}) S_0(t) + k_1 D_0^+(t) + k_\mathrm{T} T_1(t) + k_{13} D_0^-(t)$$

$$\frac{\mathrm{d}}{\mathrm{d}t} D_0^-(t) = -(k_{13} + k_{14}) D_0^-(t) + k_4 T_1(t) + k_3 S_0(t)$$

This last step of combining rates $k_{i\mathrm{a}}$ and $k_{i\mathrm{b}}$ of transitions to states of the same charge and the same multiplicity, illustrates that it is very easy to include further higher-lying states at a later stage. Conversely, some transitions never occur in the actual experiments. Transition 14, for example, does not occur during the sweep pulse, since the experiments did not include initialization in D_0^-. Population of D_0^- can therefore only occur for voltages, for which D_0^- is energetically below T_1, such that transition 14 is energetically not accessible during the sweep pulse.

Before discussing the rate equations further below, we will first consider in general which transitions can occur during the pump-probe pulse sequence as a result of the tunneling of one, and only one electron. For example, the transition from D_0^+ to a neutral excited triplet state, which has two electrons in the HOMO and one electron in each LUMO and HOMO-1 (ref. 9) would require concerted tunneling of more than one electron. Such a process is very unlikely and therefore expected to be invisible here. However, many of the states are expected to have multi-reference character[9-11]. For example, the excited triplet state described above is expected to strongly interact via pair-hopping (the concerted hopping of two electrons in Fock space) with another neutral excited triplet state, which has one electron in each the HOMO and the LUMO+1. This latter state will be accessible from D_0^+ by tunneling of a single electron. Likewise, the neutral excited singlet state having two electrons in the LUMO and none in the HOMO was found to have a non-zero contribution of a configuration with two electrons in the HOMO and none in the LUMO, as elaborated in SI section 12. If such multi-reference character is present, it is enough that one contributing many-body state is accessible to be observed in our experiment. Nevertheless, we cannot rule out that some excited states might be invisible in the spectra.

The above set of rate equations can be written in a compact form by bringing the time-dependent populations in vector form as $\boldsymbol{P} = (D_0^+, T_1, S_0, D_0^-)$, such that

$$\frac{\mathrm{d}}{\mathrm{d}t} \boldsymbol{P}(t) = K \boldsymbol{P}(t),$$

$$\text{with } K = \begin{bmatrix} -(k_1 + k_2) & k_{12} & k_{11} & 0 \\ k_2 & -(k_4 + k_{12} + k_\mathrm{T}) & 0 & k_{14} \\ k_1 & k_\mathrm{T} & -(k_3 + k_{11}) & k_{13} \\ 0 & k_4 & k_3 & -(k_{13} + k_{14}) \end{bmatrix},$$

having the solution

$$\boldsymbol{P}(t_\mathrm{sweep}) = \exp(K t_\mathrm{sweep})\boldsymbol{P}(t = 0).$$

This solution has been used to calculate the final populations numerically and fit the data. The initial populations $\boldsymbol{P}(t = 0)$ are those present at the beginning of the sweep pulse, that is, after preparing the molecule with the set pulse. In case of the data shown in Figs. 3 and 5a, the set pulse brings the molecule to D_0^+, such that it was assumed that the molecule was always in D_0^+ at the start of the sweep pulse, hence $\boldsymbol{P}(t = 0) = (1, 0, 0, 0)$. In contrast, in case of the data of Figs. 4 and 5d, the molecule was brought to either S_0 or T_1 by a set pulse sequence. In this case, it was assumed that the molecule was in one of these two states, and the initial fraction in T_1 was used as a fitting parameter (note that this parameter is directly reflected in the value of the plateau between voltages of (8) and (3B), such that there is little ambiguity in fitting this parameter).

Fitting the data numerically, as described above, is relatively slow. To systematically scrutinize the fitting procedure in many fit runs under varying conditions, approximate analytical solutions of the above differential equations were used. However, the final fit was performed numerically.

All rates except for k_T (and except for the immediate transitions, see above) involve a tunneling event between tip and molecule. Whether a given tunneling process is possible, depends on the applied voltage. Tunneling of an electron into the molecule becomes possible above a certain threshold voltage, while tunneling of an electron from the molecule into the tip becomes possible below a threshold voltage. The phonon-broadened states are observed in conventional scanning tunneling spectroscopy as Gaussian peaks in the differential conductance[12], corresponding to an onset of the tunneling rate with voltage as an error function[13], which is also used here for the fitting. Finally, the tunneling probability is also a function of applied voltage, as the latter affects the effective barrier height for tunneling. As the spectra acquired here typically cover a range of several volts, the effective barrier height can vary considerably. To include this effect in the fits, the WKB approximation of tunneling through a trapezoidal barrier is used[14]. This results in the following form for the tunneling rates k_i:

$$k_i = k_{i0} \exp\left(-2\frac{2\sqrt{2m}}{3\hbar}\frac{\left(\varphi_m^{\frac{3}{2}} - \varphi_t^{\frac{3}{2}}\right)}{\varphi_m - \varphi_t} d \right)\left(1 + \mathrm{erf}\left(\pm\frac{V_\mathrm{G} - V_i}{w_i}\right)\right)/2,$$

with the electron mass m, the reduced Planck constant $\hbar$, the tunneling distance d, the applied gate voltage V_G, the molecule-sided barrier height $\varphi_\mathrm{m} = \Phi_\mathrm{s} - \alpha V_i$, and the tip-sided barrier height $\varphi_\mathrm{t} = \Phi_\mathrm{t} - \alpha(V_i - V_\mathrm{G})$, with the lever arm α and the work functions of the sample Φ_s and tip Φ_t (see Fig. S6b). k_{i0}, V_i, and w_i are the three fit parameters for every transition i, describing the

reference rate, the voltage threshold and the width of the phonon-broadened states, respectively. The full width at half maximum can be derived from the w_i values by multiplication with $2\sqrt{\ln(2)}$. On the sample side of the junction, a derivation of the tunneling probability based on the specific molecular orbitals would be more appropriate, but this would require an *a-priori* assignment of molecular orbitals to each transition. The WKB approximation as presented above works without such presumptions and was therefore preferred. Differences in tunneling rate of other origins that do not depend on voltage, as e.g. the multiplicity of the states, their individual spin-state overlap (some examples are discussed in section 1), and the lateral dependence of wave-function overlaps are accounted for by different k_{i0}, which serve as fitting parameters. For tunneling into the molecule and out of the molecule the sign in front of the argument of the error function (erf) is positive and negative, respectively.

For large negative voltages V_G, the tip-sided barrier height $\varphi_t = \Phi_t - \alpha(V_i - V_G)$ can become negative (see Fig. S6c)[15]. In this situation the above equation takes a different form, i.e.,

$$k_i = k_{i0} \exp\left(-2\frac{2\sqrt{2m}}{3\hbar}\frac{\varphi_m^{\frac{3}{2}}}{\varphi_m - \varphi_t}d\right)\left(1 + \mathrm{erf}\left(\pm\frac{V_G - V_i}{w_i}\right)\right)/2.$$

The lever arm α, the work functions Φ_s and Φ_t and the tunneling distance d were not used as fit parameters. α was set by gauging the S_0-S_1 energy difference of pentacene against literature values as described in the main text. The work functions of tip and sample were both set to 4 eV. The tunneling distance d was found empirically to yield a good fit for d = 9 Å.

At first glance, the fixed choices for these quantities might seem arbitrary and therefore require a discussion. First of all, the values are reasonable estimates: The substrate Ag(111) has a work function of 4.74 eV (ref. 16) and it is known that NaCl reduces the work function by roughly 1 eV (ref. 17 and 18). Kelvin probe spectroscopy data directly reveal the work function difference between tip and sample, which we measured to be small compared to 4 eV (see contact potential difference in Table S1). The experimental tunneling distance d was estimated to be 9 Å from the experimentally known difference between the tip height used in the spectra and the tip height required for bond-resolved imaging with a CO-functionalized tip[19]. For the latter, a good estimate of the tip-molecule distance exists[20]. This value of 9 Å matches the tunneling distance found empirically to yield a good fit.

In the above equations one could simply omit the exponential term describing the tunneling probability, while the error function would still provide a reasonable fit to the step-like features in the spectra yielding the desired parameters, namely a set of V_i. The exponential term is included to obtain the explicit voltage dependence of the tunneling probability, which expresses itself in the slight voltage dependent populations between the step-like features, see for example Fig. 5. Including the voltage dependence of the tunneling probability improves the fit considerably, as shown in Figs. S9a and b. However, the precise choice of barrier height and width (within reasonable bounds) is much less important for the quality of the fit (see Fig. S9). Likewise, it is unimportant for the fit, whether the barrier is slightly larger at its left flank than at the right, or the other way around. Therefore, we set the work functions to reasonable values, neglect the difference in work functions between tip and sample, and set the tunneling-barrier width such that the voltage-dependent populations between the step-like features in the spectra are reproduced well.

Yet, a difference in work function of tip and sample, i.e. a non-zero CPD, has another effect. A non-zero CPD will result in an electric field in the junction even at zero gate voltage. The

voltage drop across the vacuum will be $(1 - \alpha)V_{CPD}$ at $V_G = 0$, and it will contribute as a constant offset to the gate voltage of $((1 - \alpha)/\alpha)V_{CPD}$. The voltage of contact potential difference V_{CPD} can be accessed by Kelvin probe force spectroscopy. This offset in the gate voltage resulting from a non-zero CPD is omitted in the equations for simplicity, since it does not affect the energy differences that we derive (because these are always acquired with one individual tip). The effect of a non-zero CPD should be taken into account when considering the absolute energies, at which the transitions happen. To this end, the V_{CPD} values for the tips used, with respect to the NaCl(> 20 ML)/Ag(111) surface, are provided in Table S1. Note that even with applied V_{CPD}, the E-field is not nullified everywhere in the junction, as the field is inhomogeneous[21]. However, also this effect from the inhomogeneous field contribution is cancelled in the energy differences considered here.

Despite the triplet decay being a triple-exponential decay, it is treated in the fit as a single-exponential decay with rate k_T as a fitting parameter for simplicity. The rate k_T is low (corresponding to a long-lived T_1 state) compared to all the considered tunneling rates k_i at the parameters of the experiment. Therefore, all sweep times used in the experiments were relatively short compared to the triplet decay. In this limited sweep-time range, the triplet decay is very well approximated by a single-exponential decay.

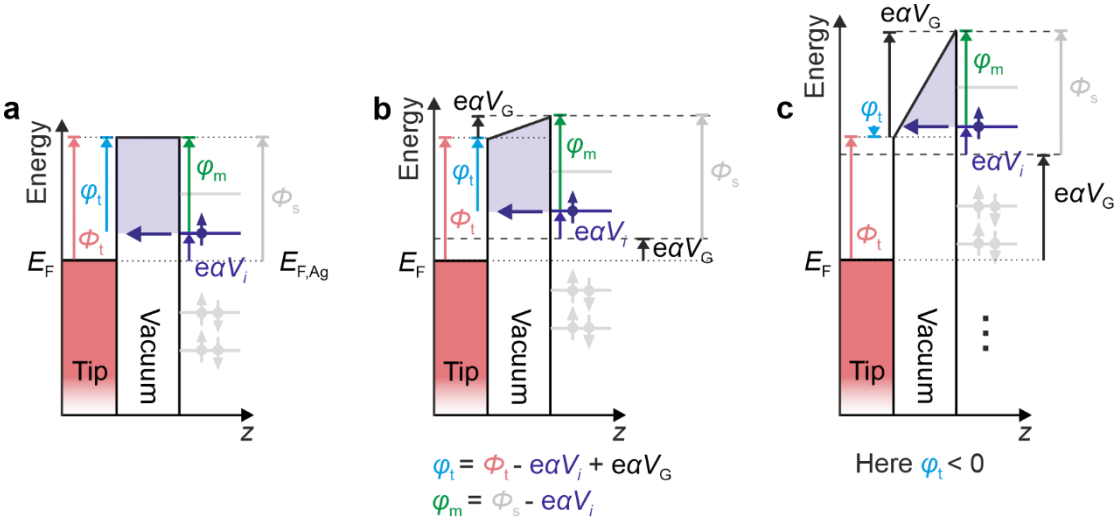

Figure S6 | Barrier height. Schematic illustration to deduce the tip-sided φ_t and molecule-sided φ_m flank of the tip-molecule tunneling barrier for a given transition with threshold voltage V_i. **a**, Taking the lever arm into account, tunneling processes occur at an energy $e\alpha V_i$ above the Fermi level of the tip E_F in absence of gating. Hence, at $V_G = 0$, φ_m and φ_t are given by subtracting $e\alpha V_i$ from the work function of the NaCl/Ag(111) substrate Φ_s and tip Φ_t, respectively. **b**, For $V_G \neq 0$, the molecular states will shift with respect to E_F by $e\alpha V_G$ (see also Fig. 1c). φ_m is not affected by the gate voltage, remaining $\varphi_m = \Phi_s - e\alpha V_i$. In contrast, φ_t changes by $e\alpha V_G$, such that we deduce $\varphi_t = \Phi_t - e\alpha V_i + e\alpha V_G$. **c**, For large negative gate voltages, φ_t can become negative, as illustrated, such that instead of the trapezoidal barrier a triangular barrier of reduced width has to be considered.

In principle, during the read-out period similar cascades of transitions as described for the sweep pulse will occur, just at a different gate voltage, the read-out voltage. However, since the read-out time is much longer than the involved tunneling rates, it can be assumed that the molecule will always return to the ground state of one of the two charge states that are brought in degeneracy by the read-out voltage. Thus, the read-out populations represent the equilibrium

limit and the fraction that is read-out in the charge state can then be expressed in terms of the populations at the end of the sweep period. For the read-out at the D_0^+-S_0 degeneracy this is

$$D^+_{0,\mathrm{read-out}} = D_0^+ + T_1 + f_{-\to+} D_0^-$$

$D^+_{0,\mathrm{read-out}}$, the read-out fraction in the D_0^+ state, is a sum of the populations in D_0^+ and T_1 as well as a fraction $f_{-\to+}$ of the population in D_0^-. Here, it is assumed that all the population in T_1 at the end of the sweep pulse will end up as D_0^+ during the read-out, since k_T is negligible against k_{12}. $f_{-\to+}$ is used as a fitting parameter; it is given by the ratio of rates k_{14} and k_{13}, where k_{14} and k_{13} also include the tunneling processes into the accessible higher-lying triplet and singlet states, respectively. Since the tunneling into S_0 has the lowest tunneling barrier (see Fig. S1), $f_{-\to+}$ is small. We indeed obtained from the fitting that $f_{-\to+}$ lies in the range of 0.03 to 0.05 for pentacene.

Analogously, for the read-out at the S_0-D_0^- degeneracy

$$D^-_{0,\mathrm{read-out}} = D_0^- + T_1 + f_{+\to-} D_0^+$$

with $f_{+\to-}$ the fraction of the population in D_0^+ that is read-out at D_0^-. This fraction is given by the ratio of rates k_1 and k_2 (including the rates into the accessible higher-lying excited singlet and triplet states). $f_{+\to-}$ is also used as fitting parameter and is found to lie in the range of 0.5 to 0.65 for pentacene. This is much larger than the values found for $f_{-\to+}$, since the tunneling barrier is in this case lowest for the highest-lying states (see Fig. S1).

8. Fitting of the pentacene and PTCDA data

The pentacene and PTCDA datasets were fitted using the equations described in section 7, taking into account the assigned transitions. Importantly, an initial guess should be made for the voltages at which the transitions occur. We estimated these initial parameters based on the experimental data, given the assignment of the transitions, as explained in the main text and in sections 1 and 3 to 6.

The pentacene data shown in Figs. 3 and 4 were fitted simultaneously using one set of parameters, resulting in the fits shown in Fig. S7.

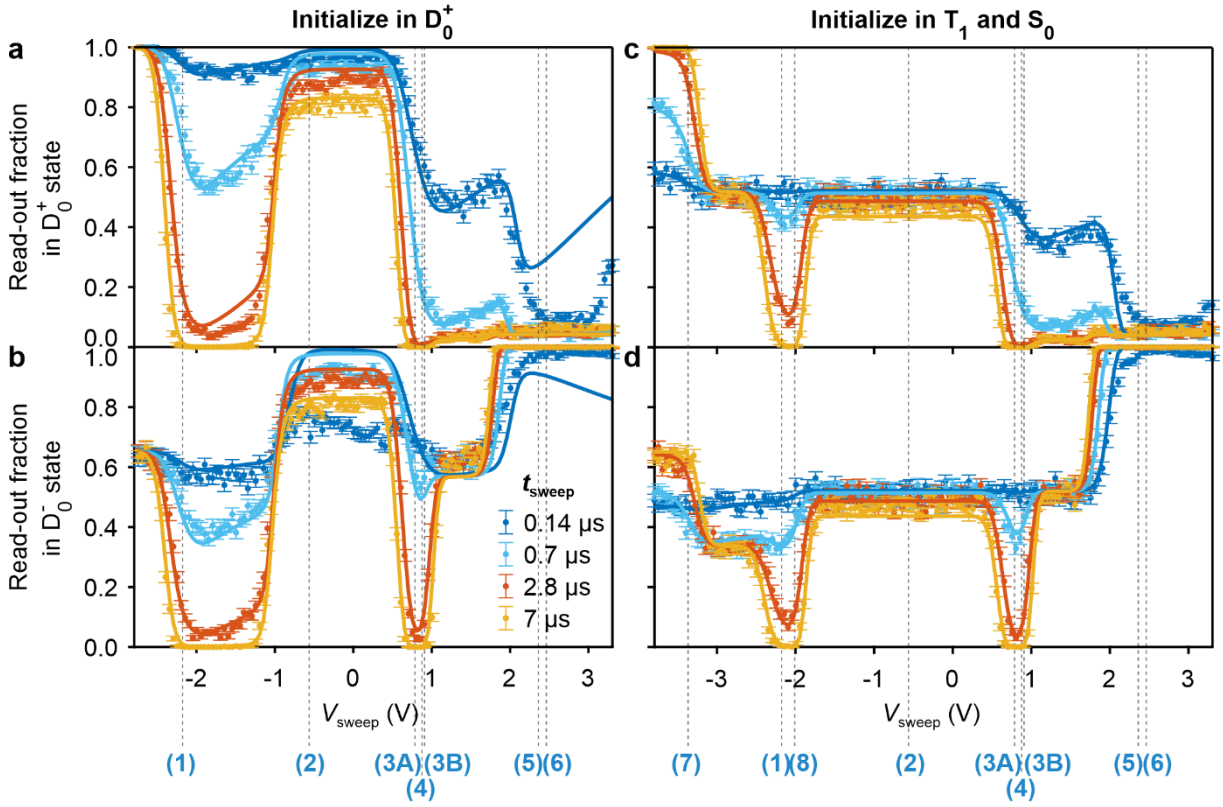

Figure S7 | Intermediate result of fitting of the excited-state spectroscopy data of pentacene. The experimental data displayed is the same as in Figs. 3 and 4 for **a**, **b** and **c**, **d**, respectively. Each data point corresponds to the normalized discrete counts of 640 pump–probe cycles and the error bars are ± s.d.; see Methods. The data was fitted using the transitions that were assigned as explained in section 1, 3 and 4 but not the $D_0^+ \rightarrow T_2$ transition that was finally included in the fitting; the solid lines represent the fits to the data. The fitted voltages of these transitions are indicated by the dotted lines and numbered analogously to Figs. 3 and 4. Three substantial discrepancies are observed between the fit and the data, which can be substantially reduced upon inclusion of the $D_0^+ \rightarrow T_2$ transition, as elaborated in the text.

Although the fit resembles the data overall very well, there are a few pronounced deviations between the fitted curves and the measured data points. These deviations are neither surprising nor alarming, since not all possible low-energy transitions have been accounted for. However, since such deviations can also influence the voltage at which the transitions of interest are fitted, we added an additional transition to improve the fit. To this end, we first identify the largest deviations, namely,

I. around (6) for the initialization in D_0^+ (Fig. S7a, b) for short t_{sweep} (dark blue graph),
II. between (2) and (3A) most pronounced for short t_{sweep} (especially the dark blue graph) for initialization in D_0^+ and read-out at the S_0-D_0^- hysteresis (Fig. S7b), and
III. the plateau after (3B) for initialization in D_0^+ and read-out at the S_0-D_0^- hysteresis, similarly pronounced for all t_{sweep} (Fig. S7b).

In comparison, the fit resembles the data for initialization in S_0 and T_1 (Fig. S7c, d) very well. This indicates that the deviations of the fit for initialization in D_0^+ can likely be solved by adding one or more transitions that start in D_0^+. As a first trial, we added the $D_0^+ \rightarrow S_2$ transition, which is expected to improve at least deviation I. As can be seen in the resulting fit in Fig. S8a, b, adding this transition considerably improved the fit with respect to deviations I and III, but did not remove deviation II. Moreover, it introduced some new deviations. As a second trial, we added a $D_0^+ \rightarrow T_2$ transition instead of the aforementioned $D_0^+ \rightarrow S_2$ transition, which results in the fit shown in Fig. S8c, d. Since this fit resembles the data very well, we concluded that the assignment as a $D_0^+ \rightarrow T_2$ transition is correct. Interestingly, at a different lateral tip position (see Fig. S2b), we also found a signature of such a $D_0^+ \rightarrow T_2$ transition - around the corresponding threshold voltage.

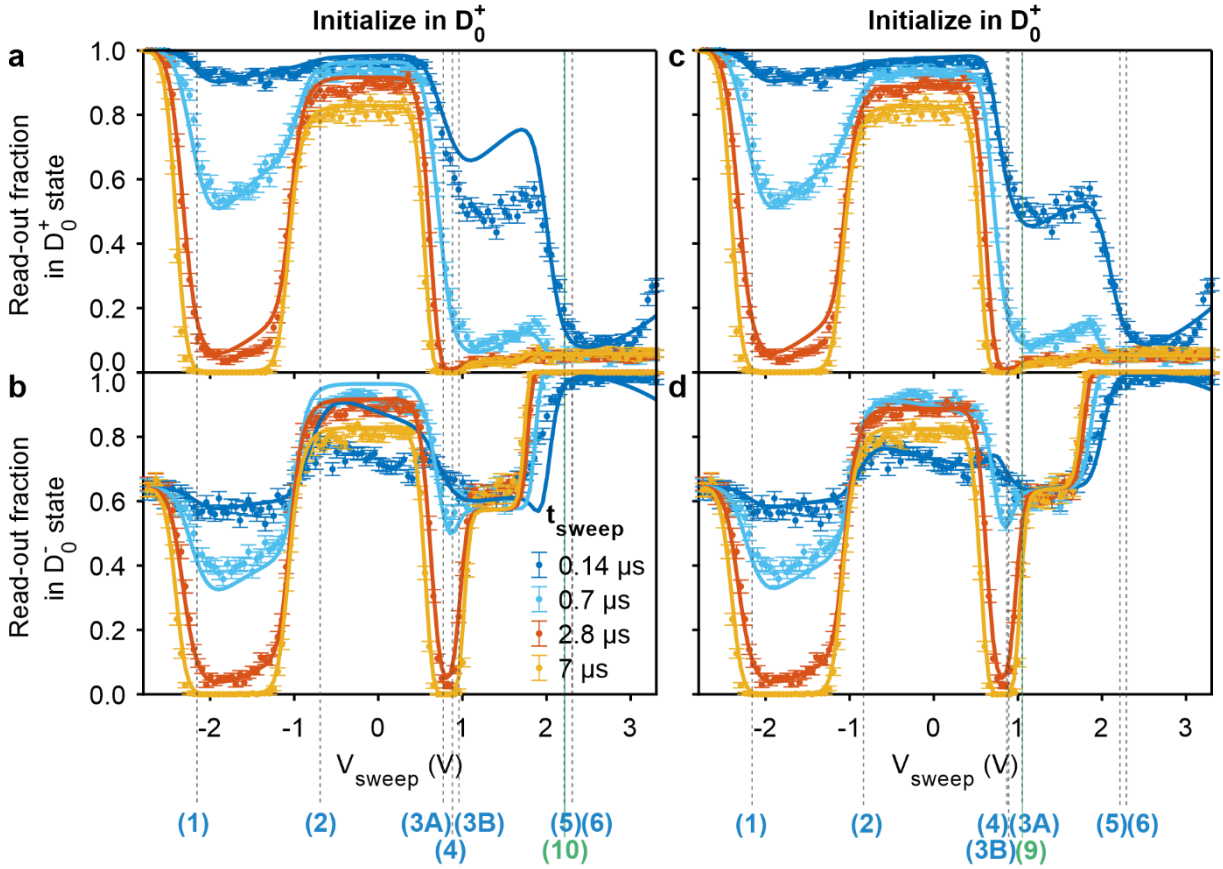

Figure S8 | Intermediate and final result of fitting of the excited-state spectroscopy data of pentacene. The experimental data displayed is the same as in Fig. 3 and Fig. S7. Each data point corresponds to the normalized discrete counts of 640 pump–probe cycles and the error bars are ± s.d.; see Methods. This data (including the spectra with initialization in T_1 and S_0) was fitted using the transitions that were assigned as explained in section 1, 3 and 4, and used in Fig. S7, but including one

additional transition (green): $D_0^+ \rightarrow S_2$ (10) in case of **a**, **b** and $D_0^+ \rightarrow T_2$ (9) in case of **c**, **d**. The fitted voltages of the transitions are indicated by the dotted lines and numbered analogously to Fig. 3. Clear discrepancies between the fit and data exist for **a**, **b**, which are not present for **c**, **d**. Therefore, a $D_0^+ \rightarrow T_2$ transition (9) was included in the final fits.

Table S1 lists the resulting fitting values for this fit including the $D_0^+ \rightarrow T_2$ transition (listed as pentacene 1). The fitted voltages at which the transitions occur are displayed for every transition, with error bars given by the uncertainty provided by the fitting algorithm. In addition, we manually estimated the error bar on the fit of a well-resolved transition (without any close-lying transitions) by varying the parameters, and find an uncertainty of ± 0.05 V, which was set as a lower limit of the uncertainties. Table S1 also lists the other fitting parameters as well as the local contact potential difference for the used tip. From the determined transition voltages and reorganization energies (see Table S2) one can also infer the values of electron affinity and ionization potential.

To understand the influence of the voltage dependence of the tunneling rates on the quality of the fit, we fitted the data neglecting (Fig. S9a) and including (Fig. S9b) the voltage dependence in the equations. This comparison demonstrates that the fitting improves significantly upon including the voltage dependence of the tunneling rates. As discussed in section 7, the strength of the voltage dependence depends on the work function and tunneling distance, which were set to 4 eV and 9 Å, respectively. As demonstrated in Fig. S9c and d, varying the work function by 1.5 eV or the distance by 3 Å does not significantly affect the fit. In fact, the resulting values of the transitions voltages for the fits shown in Figs. S9b, c and d are equal within their uncertainty margins.

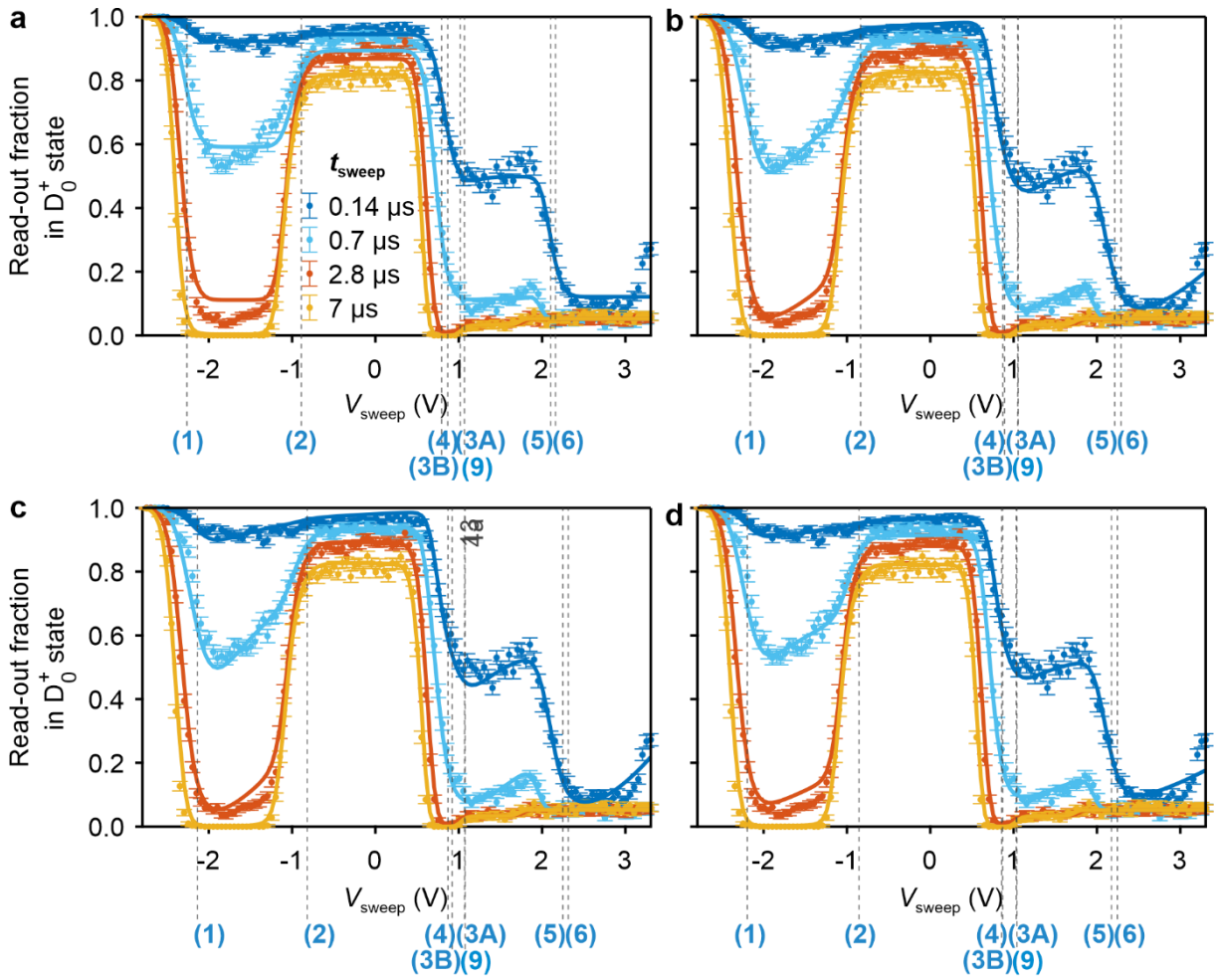

Figure S9 | Effect of the voltage dependence of the tunneling rates on the fitting. The experimental data displayed is the same as in Fig. 3a and was fitted with the same transitions as in Figs. S8c and d. Each data point corresponds to the normalized discrete counts of 640 pump–probe cycles and the error bars are ± s.d.; see Methods. Since the gate voltage changes the effective barrier height, the tunneling rates will depend on the gate voltage, which we take into account using a WKB model (see section 7). **a**, Fit neglecting the voltage dependence. **b**, Fit including the voltage dependence, using $\Phi = 4$ eV and $d = 9$ Å (as used throughout this manuscript). **c**, **d**, Influence of varying the work function and tunneling distance on the fitting: **c**, $\Phi = 2.5$ eV and $d = 9$ Å, **d**, $\Phi = 4$ eV and $d = 6$ Å. The fitted voltages of the transitions are indicated by the dotted lines and numbered analogously to Fig. 3.

Further insight into the uncertainties is provided by the data measured for three other pentacene molecules (all measured with another microtip), which were similarly fitted including the $D_0^+ \rightarrow T_2$ transition. The resulting values are also listed in Table S1. Note that for two of these pentacene molecules, spectra were only measured for read-out at the D_0^+-S_0 degeneracy, not for read-out at the S_0-D_0^- degeneracy. In these cases, the transitions $D_0^- \rightarrow S_0$ and $S_0 \rightarrow D_0^-$ only had a small influence on the spectra and could not be reliably fitted. For the fitting to converge, the fitting parameters of these transitions had to be fixed, and they were fixed to the parameters obtained for pentacene molecule 1 (correcting for the overall shifts of all transition voltages for these two molecules by comparing the transition voltages of the $D_0^+ \rightarrow S_0$ transition).

The data for PTCDA was fitted analogously. Next to the data shown in Fig. 5, a dataset was included with initialization in D_0^+ and read-out at the S_0-D_0^- hysteresis (see Fig. S10). In case

of PTCDA, the $D_0^+ \rightarrow T_2$ transition was included in the fitting from the beginning, since this transition was already assigned, as described in section 5. The resulting fits are shown in Fig. 5 and S10 and the resulting fitting values in Table S1. The large uncertainty of the $S_0 \rightarrow D_0^-$ transition is likely a result of the limited amount of data that was included for read-out at the D_0^- state (e.g. lack of data for initialization in T_1 and S_0).

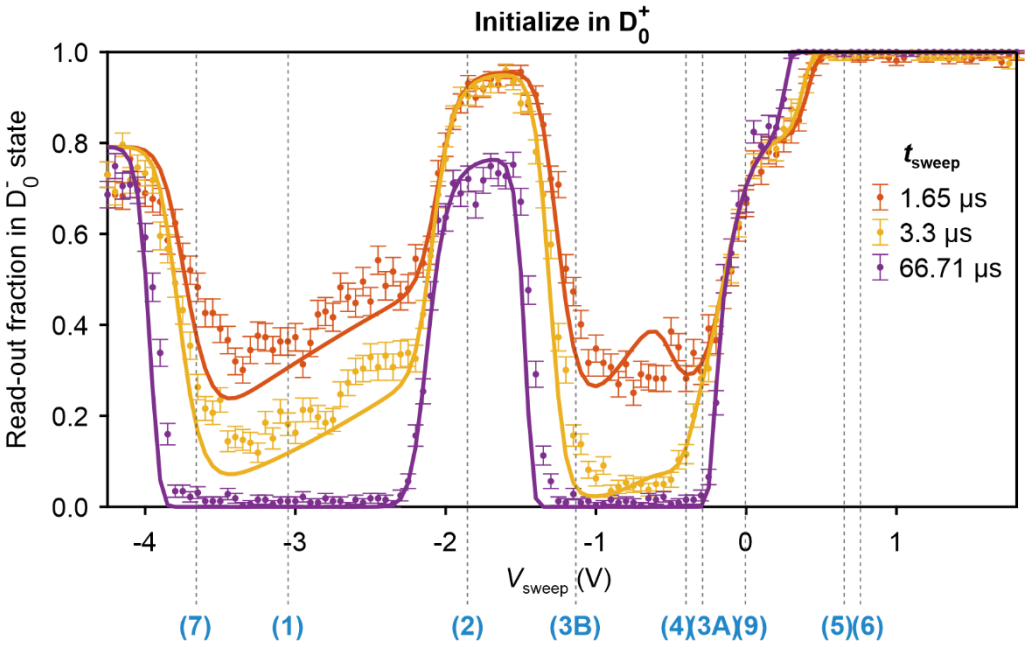

Figure S10 | Fitting of the excited-state spectroscopy data of PTCDA. Excited-state spectroscopy for the same individual PTCDA molecule as the one of the spectra shown in Fig. 5. Measurements were performed with a voltage pulse sequence similar to Fig. 2a, with a set pulse to initialize the molecule in D_0^+ (V_{set} = -5.30 V) and read-out at the S_0-D_0^- degeneracy ($V_{read\text{-}out}$ = 0.058 V). The voltage-pulse sequence was repeated 4 times per second for 80 seconds. Each data point corresponds to the normalized discrete counts of the resulting 320 pump–probe cycles and the error bars are ± s.d.; see Methods. The data was fitted using the transitions that were assigned as explained in section 5; the solid lines represent the fits to the data. The fitted voltages of these transitions are indicated by the dotted lines and numbered analogously to Figs. 3, 4 and S4.

We reiterate that this additional $D_0^+ \rightarrow T_2$ transition was only included to improve the fitting of the main transitions. Further, we fitted the data using a minimal number of transitions, but more transitions could be present that coincide with other transitions and are therefore not clearly visible. For instance, additionally including a $D_0^+ \rightarrow T_3$ transition as well as a $D_0^+ \rightarrow S_2$ transition in the fit for pentacene around the voltage where the $D_0^+ \rightarrow T_3$ transition is observed at a different spatial location (see Fig. S2b) fits the data similarly well. In case of PTCDA, for instance including $D_0^+ \rightarrow S_2$ and/or $D_0^+ \rightarrow S_3$ transitions provides fits of similar quality.

Table S1 | Fitting results for four pentacene molecules and a PTCDA molecule

	Pentacene 1	Pentacene 2	Pentacene 3	Pentacene 4	PTCDA 1
Transition voltage (V)					
$D_0^+ \rightarrow S_0$	-2.16 ± 0.05	-2.02 ± 0.05	-2.05 ± 0.05	-1.70 ± 0.05	-3.66 ± 0.05
$D_0^+ \rightarrow T_1$	-0.84 ± 0.05	-0.75 ± 0.05	-0.70 ± 0.05	-0.56 ± 0.05	-1.86 ± 0.05
$D_0^+ \rightarrow S_1$	1.05 ± 0.06	1.17 ± 0.05	1.30 ± 0.11	1.29 ± 0.07	-0.29 ± 0.05
$D_0^+ \rightarrow T_2$	1.05 ± 0.07	1.13 ± 0.06	1.35 ± 0.10	1.16 ± 0.07	0.00 ± 0.05
$T_1 \rightarrow D_0^-$	0.89 ± 0.05	1.05 ± 0.05	0.92 ± 0.05	1.08 ± 0.05	-1.13 ± 0.05
$T_1 \rightarrow D_1^-$	2.29 ± 0.05	2.48 ± 0.05	2.37 ± 0.05	2.36 ± 0.10	0.76 ± 0.05
$D_0^- \rightarrow S_0$	0.87 ± 0.05	-	0.90 ± 0.20	-	-0.40 ± 0.05
$S_0 \rightarrow D_0^-$	2.21 ± 0.05	-	2.25 ± 0.05	-	0.65 ± 0.87
$T_1 \rightarrow D_0^+$	-2.01 ± 0.05	-1.97 ± 0.13	-1.90 ± 0.05	-1.60 ± 0.09	-3.05 ± 0.05
$S_0 \rightarrow D_0^+$	-3.37 ± 0.05	-3.32 ± 0.05	-3.34 ± 0.07	-2.92 ± 0.05	-4.97 ± 0.09
Other					
T_1 decay rate (μs^{-1})	0.017 ± 0.001	0.015 ± 0.001	0.027 ± 0.002	0.020 ± 0.003	0.0034 ± 0.0003
$f_{-\rightarrow+}$	0.052 ± 0.003	0.030 ± 0.006	0.049 ± 0.006	0.055 ± 0.006	0.031 ± 0.006
$f_{+\rightarrow-}$	0.644 ± 0.004	-	0.526 ± 0.008	-	0.79 ± 0.02
Initial T_1 population	0.518 ± 0.002	0.514 ± 0.005	0.514 ± 0.004	0.510 ± 0.006	0.791 ± 0.006
Lever arm α	0.70 ± 0.02	0.71 ± 0.02	0.67 ± 0.03	0.76 ± 0.03	0.71 ± 0.03
V_{CPD} (V)	-0.47 ± 0.01	-0.42 ± 0.02	-0.46 ± 0.02	-0.57 ± 0.05	-0.42 ± 0.02

The results of the fitting for five datasets measured for four pentacene molecules and one PTCDA molecule are listed. The error bars are given by the uncertainty on the fit, with a minimal error bar on the transition voltages set to 0.05 V. The voltages of local contact potential difference (V_{CPD}) were determined as the maximum of a Kelvin probe force spectroscopy parabola measured above the molecule. The lever arm was determined as discussed in section 9.

The uncertainty on the fit of some of the transitions is much larger than on the others, which we attribute to the presence of multiple transitions around the same voltage. Another complication is that in some cases the fit could compensate a too large width of a transition by using a larger rate. Since the widths of all the transitions that do not show this behavior are similar and around 0.20 V for pentacene and 0.17 V for PTCDA (FWHM 0.33 and 0.28 V, respectively), we set a slightly larger upper limit for all widths w_i: 0.25 V and 0.20 V, respectively. To understand if such an upper limit might affect the corresponding threshold voltages, we varied the upper limit by 0.05 V. While this did affect some fitted threshold voltages, these shifts were within the uncertainty margins and hence insignificant.

The provided values of pulse durations correspond to the ones set at the driving electronics. However, the wiring in the apparatus to the sample acts as a low-pass filter, effectively shortening the pulse durations by a fixed amount. Correspondingly, we found that the fit is improved if we subtract 40 ns from all pulse durations for the fit; 40 ns seems in reasonable agreement with the expected settling time of the circuit.

9. Determination of the lever arm

The determined transition voltages have to be rescaled to energies based on the lever arm[13,22] of the gate, as follows. Due to the thick NaCl film used, part of the voltage will drop across the NaCl. This voltage drop could be estimated as shown in literature[13], but is subject to large uncertainty margins due to the uncertainty on the tip-NaCl distance, the tip radius and the local thickness of the NaCl film. Instead, we calibrate our energies using the S_0-S_1 energy difference determined as 2.26 eV by STM-induced luminescence for pentacene on NaCl(4 ML)/Ag(100) (ref. 7). We believe that this value of the S_0-S_1 energy difference is the most reliable to be taken as a reference value, due to the similarity in the environment of the molecule (i.e. NaCl as a surface, presence of a Ag metal tip). Since the lever arm α also affects the effective barrier heights (see section 7), it was set iteratively for the pentacene datasets such that the S_0-S_1 energy difference was derived as 2.26 eV. We, thereby, estimate a voltage drop of 30% in the NaCl film for the data shown in Figs. 3 and 4, corresponding to a lever arm $\alpha = 0.70$.

The uncertainty of this estimated voltage drop arises from the uncertainty on the fitting of the S_0-S_1 energy difference, as well as the uncertainty on the comparison of the S_0-S_1 energy differences in slightly different environments. For instance, the different thicknesses of the NaCl layer, and thus a different proximity of the metal underneath the NaCl can cause shifts on the order of at least tens of meV (ref. 23). Furthermore, the difference in electric field in the tip-sample junction for the luminescence measurements compared to our spectroscopic measurements of the $D_0^+ \rightarrow S_0$ and $D_0^+ \rightarrow S_1$ transitions will cause a slight deviation between our determined value and the 2.26 eV obtained with STM-induced luminescence. A change in electric field during the STM-induced luminescence measurements on pentacene caused a Stark shift of the S_1-S_0 transition of less than 10 meV/V (ref. 7). We estimated the uncertainty due to differences in the environment including the applied electric field to be 50 meV. Taking the sources of uncertainty on the lever arm together, we estimate that the resulting uncertainty of the lever arm is ± 0.02.

Since the lever arm depends on the local thickness of the salt, it was determined individually for every pentacene molecule that was measured. Similar level arms were obtained ranging from 0.67 to 0.76, as listed in Table S1.

In case of the lever arm for PTCDA, the same value was taken as determined for the pentacene molecule that was co-adsorbed on the same NaCl terrace (pentacene 2), since the lever arm depends on the thickness of the NaCl layer. In this case, the uncertainty on α was increased to account for possible slight variations in the lever arm for the two measurements, which could result from a slightly different tip height, or minor differences in the adsorption height of the molecules[13]. This additional uncertainty was estimated to be ± 0.02.

10. Energy differences, reorganization energies, line widths and rates of the transitions

As mentioned in the main text, the energy differences were derived by taking the difference between the threshold voltages of two transitions starting at the same state and ending in the two states of interest (e.g. $D_0^+ \rightarrow S_0$ and $D_0^+ \rightarrow T_1$ for the S_0-T_1 energy difference), rescaling the result by the lever arm (section 9). The results for the four pentacene molecules and one PTCDA molecule are listed in Table S2. The uncertainty margins for the individual molecules were derived from the uncertainties of the transition voltages and the uncertainty on the lever arm (see Table S1). The uncertainties on the averaged values for pentacene were determined from the standard deviation on the four individual values, taking the uncertainty on the comparison between the fitted S_0-S_1 energy differences and the literature value[7] (see section 9) into account.

Our excited-state spectroscopy provides also direct access to the reorganization energies involved in the charge-state transitions. The reorganization energies are given by the difference of energies, at which two opposing charge transitions occur, for example (1) and (7) for $D_0^+ \leftrightarrow S_0$. From the fitting of the four pentacene datasets, the reorganization energies of $D_0^+ \leftrightarrow S_0$, $D_0^+ \leftrightarrow T_1$ and $S_0 \leftrightarrow D_0^-$ were derived as (0.89 ± 0.07) eV, (0.82 ± 0.07) eV and (0.93 ± 0.06) eV, respectively (see Table S2). The uncertainty margins were derived analogously as for the energy differences (see above). The $S_0 \leftrightarrow D_0^-$ value matches the value of (0.9 ± 0.1) eV as obtained from density-functional theory calculations[24].

Table S2 | Derived energies for pentacene and PTCDA

	Pentacene 1	Pentacene 2	Pentacene 3	Pentacene 4	Average	PTCDA 1
Energy difference (eV)						
T_1-S_0	0.93 ± 0.06	0.90 ± 0.06	0.91 ± 0.06	0.86 ± 0.06	0.90 ± 0.06	1.28 ± 0.07
S_1-S_0	2.26 ± 0.09	2.26 ± 0.09	2.26 ± 0.12	2.26 ± 0.10	2.26 ± 0.05	2.39 ± 0.11
D_1^--D_0^-	0.99 ± 0.06	1.01 ± 0.06	0.98 ± 0.06	0.97 ± 0.09	0.99 ± 0.04	1.34 ± 0.08
T_2-S_0	2.26 ± 0.09	2.23 ± 0.09	2.29 ± 0.12	2.17 ± 0.10	2.24 ± 0.12	2.59 ± 0.12
Reorganization energy (eV)						
D_0^+-S_0	0.85 ± 0.06	0.92 ± 0.06	0.87 ± 0.07	0.92 ± 0.06	0.89 ± 0.07	0.93 ± 0.08
D_0^+-T_1	0.83 ± 0.06	0.86 ± 0.10	0.81 ± 0.06	0.78 ± 0.08	0.82 ± 0.07	0.85 ± 0.06
S_0-D_0^-	0.95 ± 0.06	-	0.91 ± 0.15	-	0.93 ± 0.06	0.75 ± 0.62 [1]

Energy differences and reorganization energies determined for different transitions for four pentacene molecules and one PTCDA molecule. The uncertainties were determined as described in the text. PTCDA 1 is lying on the same NaCl terrace as pentacene 2 (see Extended Data Fig. 3), therefore, the lever arm determined for pentacene 2 was used to rescale the values for PTCDA 1 (see section 9). [1] The large uncertainty of the S_0-D_0^- reorganization energy for PTCDA 1 is likely a result of the limited amount of data that was included for read-out at the D_0^- state (e.g. lack of data for initialization in T_1 and S_0).

The similar reorganization energies for the three different transitions found here, strongly support the assumption that the relaxation energies are similar for the transitions under consideration. This assumption is used in the derivation of the energy differences. Further support for the validity of this assumption can be derived from the similar widths of the different transitions. These widths arise from the same strong electron-phonon coupling that is also the

cause of the large relaxation energies[12]. We find similar widths for the transitions that are involved in our derivation of the energy differences, in the range of 0.15 to 0.18 eV (FWHM 0.24 to 0.30 eV), lending further support that the relaxation energies are similar.

Analogously, in case of PTCDA, the reorganization energies were extracted as (0.93 ± 0.08) eV for $D_0^+ \leftrightarrow S_0$, (0.85 ± 0.06) eV for $D_0^+ \leftrightarrow T_1$ and (0.75 ± 0.62) eV for $S_0 \leftrightarrow D_0^-$. Thus, also for PTCDA, the reorganization energies are similar. Also the widths of the transitions involved in the derivation of the energy differences are similar, in the range of 0.13 to 0.14 eV (FWHM 0.22 to 0.23 eV).

The reorganization energies of the short-lived excited states cannot be accessed since transitions from such a state into another state are not observed. The corresponding relaxation energies for pentacene displayed in Fig. 6 are shown as half of the mean values of the reorganization energies listed above. For PTCDA we proceeded analogously but disregarded the value of the reorganization energy of the S_0-D_0^- transition due to its large uncertainty.

The assumption of similar relaxation energies is further justified by the similar confinement of the frontier orbitals involved in the transitions considered here for pentacene and PTCDA. However, if – for other molecules - the orbital confinement greatly differs for different states, different relaxation energies should be considered. In such cases the relaxation energies for injecting and removing an electron into and out of one given orbital is still expected to be approximately the same. The relaxation energies can, therefore, be estimated from the reorganization energy, being the sum of these two relaxation energies. As mentioned above, the relaxation energies and the widths of the involved transitions scale in a well-defined manner[12] and provide another way to separately extract relaxation energies for such cases.

The relative rates (not listed) can be interpreted semi-quantitatively. While the fitted threshold voltages vary only slightly when adding more possible transitions to the fitting procedure, the fitted rates show a much larger dependence. Similarly, the relative rates depend strongly on the tip position, reflecting different orbital density distributions. The latter can aid the assignment of features to certain transitions.

The relative rate constants are also reflected in the $f_{+\rightarrow-}$ and $f_{-\rightarrow+}$ parameters, as well as the initial T_1 population listed in Table S1. For instance, the initial T_1 population (after the usedset pulse sequence to initialize in T_1 and S_0) is determined by the ratio of $D_0^+ \rightarrow T_1$ and $D_0^+ \rightarrow S_0$ as well as the triplet decay rate. The fitted initial T_1 populations are almost equal within their error margins for the four pentacene molecules. A slightly larger spread is found for $f_{+\rightarrow-}$ and $f_{-\rightarrow+}$, which we mainly attribute to the larger number of transitions involved.

11. Extrapolation to ultrathin NaCl films

While our excited-state spectroscopy requires measuring on insulating NaCl films of sufficient thickness to prevent tunneling to the substrate, our results can be extrapolated to experiments performed on ultrathin (few monolayer) films of NaCl, guiding the interpretation of these experiments. An example of such extrapolation is given in the main text for PTCDA on 3 ML NaCl/Ag(111) guided by general considerations as follows.

The voltage applied to the substrate drops also for ultrathin films partially between molecule and substrate, which has to be taken into account. For ultrathin films it is a bias (V_B) rather than a gate voltage since it drives a net current across the junction. However, technically V_B and V_G are the same and both refer to the voltage applied to the substrate with respect to the tip. To compare our PTCDA results with the STM-induced luminescence measurements on 3 ML NaCl/Ag(111), we estimate the lever arm based on the STS and S_1-S_0 STM-induced luminescence measurements from the work we compare with, ref. 8. The lever arm was derived from the threshold voltage for LUMO imaging ($D_0^- \rightarrow S_0$) of -0.55 V and the threshold voltage for the observed S_1-S_0 luminescence (corresponding to the threshold for $D_0^- \rightarrow S_1$) of -3.3 V (ref. 8). Comparing this S_1-S_0 voltage gap of 2.75 V to the observed S_1-S_0 luminescence of 2.45 eV (ref. 8), a lever arm α of 0.89 results. In other words, 89% of the applied voltage drops between molecule and tip, while (1 - α) = 11% of the voltage drops between molecule and substrate (see Fig. S11).

On thick (> 20 ML) insulating films, only tunneling between molecule and tip is possible, and therefore, in the many-body description, the reference energy for electron tunneling is the Fermi level of the tip. In case of ultrathin films, however, not only tunneling between the tip and the molecule is possible, but also between the molecule and the metal substrate beneath the ultrathin film. This substrate tunneling will always bring the molecule back to the state(s) lowest in energy. It is therefore more convenient to choose the Fermi level of the sample as the reference energy in the many-body diagram for ultrathin films. The applied voltage shifts the molecular levels with respect to the Fermi level of the surface by $-q(1-\alpha)V_B$, with q the net charge of the molecule. This shift can possibly open up new substrate tunneling pathways, in particular, if at zero bias molecular levels are close to the Fermi level[22]; any substrate tunneling corresponds to a transition going downward in the many-body diagram in Fig. 6c. Tunneling channels to/from the tip are opened by the application of V_B, as indicated by the upward arrows (having a vertical component of up to qV_B) in the many-body diagram in Fig. 6c.

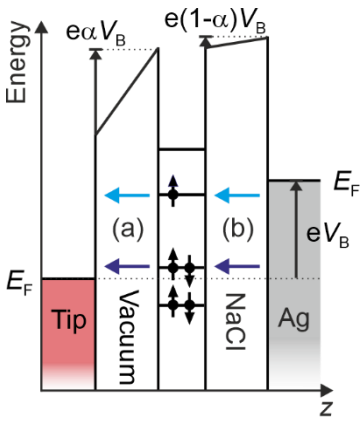

Figure S11 | Schematic of the double-barrier tunneling junction for ultrathin NaCl. An applied bias voltage V_B shifts the molecular levels with respect to the Fermi level of the tip. A part of V_B, i.e., $(1 - \alpha)V_B$, drops in the NaCl film, and the remainder, i.e., αV_B, drops in the vacuum between tip and molecule. To simplify the illustration, it implies that at $V_B = 0$ there is no electric field in the junction – without loss of generality. In the situation displayed, the applied voltage (V_B = -2.5 V) enables tunneling of an electron from the LUMO (light blue) or HOMO (dark blue) to the tip (indicated with (a)). Note that in case of PTCDA on 3 ML NaCl on Ag(111), D_0^- is the ground state (ref. 8, 29); if $V_B = 0$, no tunneling between the substrate and the LUMO of PTCDA will occur. If V_B is large enough to allow tunneling of electrons between tip and molecule, the molecule will be brought back to its ground state by substrate-molecule tunneling, indicated with (b). To understand the pathways leading to luminescence, it is better to consider the many-body picture displayed in Fig. 6c.

When extrapolating from thick to thin films, in addition, the increased screening due to polarization of the metal substrate has to be considered. This may slightly affect excitation energies (e.g. S_0-T_1 and D_0^--D_1^- energy differences). For example, a shift of a few tens of meV was observed for the S_0-S_1 energy difference of zinc phthalocyanine from 2 to 5 ML of NaCl, see ref. 23. Similarly, the possible difference in electric field present in the tip-sample junction by e.g. differences in the applied voltage can also cause slight shifts in the excitation energies via the Stark effect. For example, a shift of 30 meV/V was observed for D_1^--D_0^- luminescence of PTCDA attached to a Ag tip[25]. Since these shifts are smaller than the uncertainty margins on our derived energy differences, these effects were neglected.

There are three effects that change the relative energy of the different charge states. First, the screening due to polarization of the metal substrate will reduce the energies of the positively and negatively charged states with respect to the neutral ones. In other words, upon reducing the thickness of a thin NaCl film, a reduction of the voltage difference between $S_0 \rightarrow D_0^+$ and $S_0 \rightarrow D_0^-$ was observed[26-28]. Although this reduction was also partially attributed to the different lever arms; the effect due to polarization was found to be on the order of 0.2 eV from 2 to 4 ML of NaCl (ref. 27).

Second, changes in the work function would also affect the level alignment. Although the work function changes strongly upon the addition of NaCl to a metal surface (around 1 eV (ref. 17 and 18)), within uncertainty margins the same work function was found comparing 2 and 3 ML of NaCl on Ag(111) (ref. 27) (and also comparing 1, 2 and 3 ML on Ag(100) (ref. 18)). We, therefore, expect that the work function does not change much from 3 to more than 20 ML of NaCl on Ag(111).

Third, in case of comparing two single molecule measurements, further variations between different individual molecules caused by other variations in their environment should be taken into account. For instance, Table S1 shows that for four different pentacene molecules measured with four different microtips, the voltage at which the S_0-D_0^+ charge degeneracy was observed varied by up to 0.45 V. Note that a part of these variations can also be attributed to the different V_{CPD} of the different tips. The tip will also contribute to screening effects as mentioned above, which will then depend on the tip shape.

These three effects all change the relative energy alignment of the charged states with respect to the neutral states. To compare our experiments on PTCDA with the STM-induced luminescence measurements, we choose to take these three effects into account by calibrating the S_0-D_0^- energy-degeneracy point using the measurements from the work we compare with, ref. 8. From the conventional tunneling spectroscopy data of this reference[8], it follows that the maximum of the $D_0^- \rightarrow S_0$ transition is at V_B = -0.8 V. Taking the derived lever arm of 0.89 (see above) into account, this maximum lies at 0.71 eV above the D_0^- state (for V_B = 0 V). The relative energy alignment of the vibrational ground states of the S_0 and D_0^- states can then be derived by taking the relaxation energy into account. We estimate the relaxation energy as 0.45 eV, which corresponds to half of the average of the reorganization energies for PTCDA derived from our data. Thus, for this molecule on 3 ML NaCl/Ag(111), the D_0^- state is estimated to be 0.27 eV lower in energy than the S_0 state (for V_B = 0 V). Since the STM-induced luminescence experiments were performed at V_B = -2.5 V, the lever arm further shifts the singly negative charge states down by 0.28 eV.

12. Two-frontier-orbital modelling of the interacting Hamiltonian

The electronic structure of organic molecules as pentacene and PTCDA in the gas phase can be calculated with a wide spectrum of different methods, ranging from density functional theory and its time dependent extensions, many body perturbation theories as GW or Bethe-Salpeter[30,31], as well as quantum chemistry approaches as coupled cluster[10] or configuration interaction methods. Hubbard like minimal interacting models based on a limited number of frontier orbitals have also been adopted[32-35].

Including the effects of the environment, as for example metallic electrodes or dielectric substrates, within an ab initio approach still remains a formidable challenge[24,28]. Scanning tunneling spectroscopy on single molecules has revealed, though, the crucial interplay between the molecule and the underlying ionic salt[24,28].

We adopted here a minimalistic approach which rationalizes a large set of the experimental results within a simple interacting model. To this purpose, we notice that most of the redox as well as of the non-radiative transitions for pentacene and PTCDA discussed in the main text involve the HOMO and the LUMO of these molecules. We thus attempt to construct an interacting model only based on these two frontier orbitals and to parametrize it by means of the threshold voltages obtained from fitting the excited-state spectroscopy, as given in Table S1.

To this purpose, we consider the most complete non-relativistic interacting Hamiltonian associated to the Fock space generated by the HOMO (H) and LUMO (L) of a symmetric molecule[1]

$$\hat{H} = \sum_{i=\mathrm{H,L}} \sum_{\sigma} \epsilon_i \, \hat{n}_{i\sigma} + U_{\mathrm{H}} \, \hat{n}_{\mathrm{H}\uparrow} \, \hat{n}_{\mathrm{H}\downarrow} + U_{\mathrm{L}} \, \hat{n}_{\mathrm{L}\uparrow} \, \hat{n}_{\mathrm{L}\downarrow} + U_{\mathrm{HL}} \sum_{\sigma \, \sigma'} \hat{n}_{\mathrm{L}\sigma'} \, \hat{n}_{\mathrm{H}\sigma}$$

$$+ J \sum_{\sigma\sigma'} \hat{d}^{\dagger}_{\mathrm{H}\sigma} \hat{d}^{\dagger}_{\mathrm{L}\sigma'} \hat{d}_{\mathrm{H}\sigma'} \hat{d}_{\mathrm{L}\sigma} + J \left(\hat{d}^{\dagger}_{\mathrm{L}\uparrow} \hat{d}^{\dagger}_{\mathrm{L}\downarrow} \hat{d}_{\mathrm{H}\downarrow} \hat{d}_{\mathrm{H}\uparrow} + \hat{d}^{\dagger}_{\mathrm{H}\uparrow} \hat{d}^{\dagger}_{\mathrm{H}\downarrow} \hat{d}_{\mathrm{L}\downarrow} \hat{d}_{\mathrm{L}\uparrow} \right),$$

where $\hat{d}^{\dagger}_{i\sigma}$ creates an electron with spin σ in the i-th molecular orbital with $i = \mathrm{H}, \mathrm{L}$ and $\hat{d}_{i\sigma}$ annihilates it, $\hat{n}_{i\sigma} = \hat{d}^{\dagger}_{i\sigma} \hat{d}_{i\sigma}$ is the corresponding number operator. The single particle component of the Hamiltonian contains the energy levels ϵ_i, and, by definition, it holds $\epsilon_{\mathrm{L}} > \epsilon_{\mathrm{H}}$. We also include in the model all two-body interacting terms allowed by symmetry[1]. They are expressed in terms of the following Coulomb integrals between the (real valued) frontier orbitals,

$$U_i = \frac{e^2}{4\pi\varepsilon_0} \int d\boldsymbol{r}_1 \, d\boldsymbol{r}_2 \, \psi_i^2(\boldsymbol{r}_1) \frac{1}{\varepsilon_r |\boldsymbol{r}_1 - \boldsymbol{r}_2|} \, \psi_i^2(\boldsymbol{r}_2) \geq 0 \, ,$$

$$U_{\mathrm{HL}} = \frac{e^2}{4\pi\varepsilon_0} \int d\boldsymbol{r}_1 \, d\boldsymbol{r}_2 \, \psi_{\mathrm{H}}^2(\boldsymbol{r}_1) \frac{1}{\varepsilon_r |\boldsymbol{r}_1 - \boldsymbol{r}_2|} \, \psi_{\mathrm{L}}^2(\boldsymbol{r}_2) \leq \sqrt{U_{\mathrm{H}} U_{\mathrm{L}}} \, ,$$

[1]We refer here to any point symmetry group having only one-dimensional irreducible representation as for example D_{2h} or C_{2v} to which pentacene and PTCDA belong, when considered, respectively in the gas phase or on a substrate breaking the reflection symmetry with respect to the plane of the molecule. The HOMO and the LUMO belong to different irreducible representations. Thus, several Coulomb integrals vanish due to symmetry considerations.

$$J = \frac{e^2}{4\pi\varepsilon_0}\int d\boldsymbol{r}_1\, d\boldsymbol{r}_2\, \psi_{\mathrm{H}}(\boldsymbol{r}_1)\psi_{\mathrm{L}}(\boldsymbol{r}_1)\frac{1}{\varepsilon_r|\boldsymbol{r}_1 - \boldsymbol{r}_2|}\psi_{\mathrm{H}}(\boldsymbol{r}_2)\psi_{\mathrm{L}}(\boldsymbol{r}_2) \geq 0\,.$$

in which e is the electron charge, ε_0 the vacuum permittivity, ε_r the relative dielectric constant, ψ_i the wavefunction of the i-th molecular orbital and $\boldsymbol{r}_j$ the position of the j-th electron. The first integral yields the energy cost for the double occupation of the i-th molecular orbital. The direct Coulomb interaction between HOMO and LUMO is measured by U_{HL}. Finally, the constant J gives the strength of the exchange interaction between these orbitals. Since we are dealing with real-valued orbitals, the latter coincides also with the strength of the pair-hopping amplitude between the two frontier orbitals. The exchange and pair-hopping components of the interacting Hamiltonian are, in the order, listed in the second line of the model molecular Hamiltonian given above. The relative dielectric constant ε_r should incorporate the screening generated by the other electrons on the molecule. All Coulomb integrals, including the exchange and pair-hopping parameter J, are positive. Moreover, it holds that $U_{\mathrm{HL}} \leq \sqrt{U_{\mathrm{H}}U_{\mathrm{L}}}$. These relations, fundamental for the fitting procedure discussed below, follow from the general inequality characterizing the electrostatic energy of a generic charge density distribution f

$$\int d\boldsymbol{r}_1\, d\boldsymbol{r}_2\, f(\boldsymbol{r}_1)\frac{1}{4\pi\varepsilon_0|\boldsymbol{r}_1 - \boldsymbol{r}_2|}\, f(\boldsymbol{r}_2) = \int d\vec{q}\, \frac{\left|\tilde{f}(\boldsymbol{q})\right|^2}{\varepsilon_0|\boldsymbol{q}|^2} \geq 0\,,$$

where $\tilde{f}$ is the Fourier transform of the real valued function f. In particular, the positivity of the exchange and pair-hopping parameter J is obtained by taking $f = \psi_{\mathrm{H}}\psi_{\mathrm{L}}$. The choice $f = \psi_{\mathrm{H}}^2 - p\psi_{\mathrm{L}}^2$ with $p > 0$ relates instead the charging energies U_{H} and U_{L} to the interorbital contribution U_{HL}, leading to the relation $U_{\mathrm{HL}} \leq \sqrt{U_{\mathrm{H}}U_{\mathrm{L}}}$.

The spectrum of the model Hamiltonian calculated in the relevant subspaces with up to three electrons occupying the frontier orbitals is readily obtained. It is given by

$$E(\mathrm{D}_0^+) = \epsilon_{\mathrm{H}} \text{ and } E(\mathrm{D}_1^+) = \epsilon_{\mathrm{L}}$$

for the cationic states,

$$\begin{aligned}
E(\mathrm{S}_0) &= \epsilon_{\mathrm{H}} + \epsilon_{\mathrm{L}} + \frac{U_{\mathrm{H}} + U_{\mathrm{L}}}{2} - \sqrt{\left(\epsilon_{\mathrm{L}} - \epsilon_{\mathrm{H}} + \frac{U_{\mathrm{L}} - U_{\mathrm{H}}}{2}\right)^2 + J^2},\\
E(\mathrm{T}_1) &= \epsilon_{\mathrm{H}} + \epsilon_{\mathrm{L}} + U_{\mathrm{HL}} - J,\\
E(\mathrm{S}_1) &= \epsilon_{\mathrm{H}} + \epsilon_{\mathrm{L}} + U_{\mathrm{HL}} + J,\\
E(\mathrm{S}_2) &= \epsilon_{\mathrm{H}} + \epsilon_{\mathrm{L}} + \frac{U_{\mathrm{H}} + U_{\mathrm{L}}}{2} + \sqrt{\left(\epsilon_{\mathrm{L}} - \epsilon_{\mathrm{H}} + \frac{U_{\mathrm{L}} - U_{\mathrm{H}}}{2}\right)^2 + J^2}
\end{aligned}$$

for the neutral states, and

$$E(\mathrm{D}_0^-) = 2\epsilon_{\mathrm{H}} + \epsilon_{\mathrm{L}} + U_{\mathrm{H}} + 2U_{\mathrm{HL}} \text{ and } E(\mathrm{D}_1^-) = \epsilon_{\mathrm{H}} + 2\epsilon_{\mathrm{L}} + U_{\mathrm{L}} + 2U_{\mathrm{HL}}$$

for the anionic states.

The positivity of the exchange parameter J implies that the triplet state T_1 is energetically favored with respect to the corresponding singlet state S_1, both having one electron per frontier

orbital. The neutral singlet ground state S_0 results from the superposition of two single Slater determinants. In second quantization

$$|S_0\rangle = \left(\cos\theta\, \hat{d}^{\dagger}_{H\uparrow}\hat{d}^{\dagger}_{H\downarrow} - \sin\theta\, \hat{d}^{\dagger}_{L\uparrow}\hat{d}^{\dagger}_{L\downarrow}\right)|\Omega\rangle\,,$$

where $|\Omega\rangle$ is the reference state with doubly occupied orbitals until the HOMO-1 and empty ones starting from the HOMO. The angle θ measuring the admixture to the ground state of the doubly occupied LUMO is expressed in terms of the parameters of the model as

$$\theta = \frac{1}{2}\tan^{-1}\left(\frac{J}{\epsilon_L - \epsilon_H + \dfrac{U_L - U_H}{2}}\right).$$

If we disregard J in comparison with $\epsilon_L - \epsilon_H + \frac{U_L - U_H}{2}$, the mixing angle θ vanishes; the neutral ground state $|S_0\rangle$ reduces then to a single Slater determinant: the singlet with double occupied HOMO and eigenenergy $E(S_0) = 2\epsilon_H + U_H$. Correspondingly, the excited singlet $|S_2\rangle$ with eigenenergy $E(S_2) = 2\epsilon_L + U_L$ would have just two extra electrons in the LUMO with respect to the reference state $|\Omega\rangle$. The pair hopping is responsible for a correlated neutral ground state, which cannot be written in terms of a single Slater determinant.

We aim at fitting the parameters of this interacting model by means of the transition voltages measured in the experiment and summarized in Table S1. We discard the transitions involving the state T_2, since the latter is not included in this minimal model. The experiments yield then the following four independent energy differences:

$$E(T_1) - E(S_0) = e\alpha\left(V_{D_0^+\to T_1} - V_{D_0^+\to S_0}\right),$$

$$E(S_1) - E(S_0) = e\alpha\left(V_{D_0^+\to S_1} - V_{D_0^+\to S_0}\right),$$

$$E(D_1^-) - E(D_0^-) = e\alpha\left(V_{T_1\to D_1^-} - V_{T_1\to D_0^-}\right),$$

$$E_{add} = E(D_0^-) - 2E(S_0) + E(D_0^+) = e\alpha\left(V_{S_0\to D_0^-} - V_{D_0^+\to S_0}\right),$$

where e is the electron charge and α the level arm. The addition energy for the neutral molecule is obtained from vertical charge transitions ($S_0 \to D_0^-$ and $D_0^+ \to S_0$) which compensate for the phononic reorganization energy disregarded in the model. The latter is assumed to be the same for every charge transition as discussed in section 10 and thus does not affect the other energy differences. The anionic transition $S_0 \to D_0^-$ was not measured for pentacene 2 and 4. In those cases we have used for the transition voltage the average of the ones determined for pentacene 1 and 3.

The same energy differences given above can be related to the model's parameters by means of the following equations

$$E(T_1) - E(S_0) = U_{HL} - \frac{U_L + U_H}{2} - J + \sqrt{\left(\epsilon_L - \epsilon_H + \frac{U_L - U_H}{2}\right)^2 + J^2},$$

$$E(S_1) - E(S_0) = U_{HL} - \frac{U_L + U_H}{2} + J + \sqrt{\left(\epsilon_L - \epsilon_H + \frac{U_L - U_H}{2}\right)^2 + J^2},$$

$$E(\mathrm{D}_1^-) - E(\mathrm{D}_0^-) = \epsilon_\mathrm{L} - \epsilon_\mathrm{H} + U_\mathrm{L} - U_\mathrm{H},$$

$$E_\mathrm{add} = -(\epsilon_\mathrm{L} - \epsilon_\mathrm{H}) + 2U_\mathrm{HL} - U_\mathrm{L} + 2\sqrt{\left(\epsilon_L - \epsilon_\mathrm{H} + \frac{U_\mathrm{L}-U_\mathrm{H}}{2}\right)^2 + J^2}\,.$$

There are six unknowns and only four independent equations. Though, as to be expected, the single particle energies only appear in the equation as difference, i.e. $\epsilon_\mathrm{L} - \epsilon_\mathrm{H}$. The latter is in fact an intrinsic property of the molecule accessible despite all energies being measured with respect to the tip chemical potential. Thus, we do not fit ϵ_H and ϵ_L separately but rather their difference. We cope with the remaining excess of the unknowns by introducing the dimensionless fitting parameter β such that

$$U_\mathrm{HL} = \frac{U_\mathrm{H} + U_\mathrm{L}}{2} + \beta\frac{U_\mathrm{L} - U_\mathrm{H}}{2}$$

and solve the equations in the range $-1 \le \beta \le 1$. This assumption implies that $U_\mathrm{L} \le U_\mathrm{HL} \le U_\mathrm{H}$, where at this level the position of U_L and U_H are still interchangeable. This relation between the interaction parameters does not represent a serious limitation. It is in fact consistent with the topography of the cationic and anionic resonances, as for instance shown in Fig. S2f and g for pentacene. The latter indicate a HOMO and a LUMO sharing most of their space, with the LUMO being more extended along the longitudinal direction of the molecule. The same spatial information confirms the relation between the charging energies $U_\mathrm{L} \le U_\mathrm{H}$. We similarly argue that these conditions also hold for the case of PTCDA.

From the equations above, one readily obtains for the exchange and pair-hopping parameter

$$J = \frac{E(\mathrm{S}_1) - E(\mathrm{S}_0)}{2} - \frac{E(\mathrm{T}_1) - E(\mathrm{S}_0)}{2} > 0\,,$$

independent of β. Similarly, the direct interaction parameter U_L can be expressed

$$U_\mathrm{L} = E_\mathrm{add} + [E(\mathrm{D}_1^-) - E(\mathrm{D}_0^-)] - [E(\mathrm{S}_1) - E(\mathrm{S}_0)] - [E(\mathrm{T}_1) - E(\mathrm{S}_0)] > 0$$

We further restrict the choice of the fitting parameter β by requiring the positivity of $\epsilon_\mathrm{L} - \epsilon_\mathrm{H}$, U_H and U_HL as well as the fulfillment of the condition $U_\mathrm{HL} \le \sqrt{U_\mathrm{H}U_\mathrm{L}}$. Having satisfied these inequalities, we eventually determine β by minimizing $|U_\mathrm{H} - U_\mathrm{L}|$, motivated by the similar spatial extent of the HOMO and the LUMO observed in the images of the cationic and anionic ground state transitions. The results of the fitting procedure are summarized in Table S3.

Table S3 | Model parameters for pentacene and PTCDA

	Pentacene 1	Pentacene 2	Pentacene 3	Pentacene 4	Average	PTCDA
$\epsilon_L - \epsilon_H$	2.04 ± 0.12	1.94 ± 0.13	2.02 ± 0.17	1.95 ± 0.24	1.99 ± 0.07	2.26 ± 0.16
J	0.66 ± 0.05	0.68 ± 0.05	0.67 ± 0.07	0.70 ± 0.07	0.68 ± 0.03	0.56 ± 0.06
U_H	2.77 ± 0.15	2.72 ± 0.15	2.62 ± 0.24	2.73 ± 0.19	2.71 ± 0.09	2.58 ± 0.50
U_L	1.71 ± 0.17	1.79 ± 0.17	1.57 ± 0.27	1.75 ± 0.21	1.71 ± 0.10	1.66 ± 0.51
U_{HL}	2.18 ± 0.14	2.21 ± 0.14	2.03 ± 0.23	2.18 ± 0.17	2.15 ± 0.09	2.07 ± 0.49

Parameters for the two frontiers orbitals model of pentacene and PTCDA extracted from the transition voltages listed in Table S1. All values are expressed in eV.

These parameters imply that the S_0 states of pentacene and PTCDA have an admixture of respectively about 4.5% and 2.3% of the state with double occupation of the LUMO. The latter opens, in turn, charge transitions (e.g. $D_0^+ \rightarrow S_2$) which would be forbidden for an uncorrelated neutral ground state.

13. Supplementary references

1. Kaiser, K.; Lieske, L.-A.; Repp, J.; Gross, L. Charge-state lifetimes of single molecules on few monolayers of NaCl. *Nat. Commun.* **2023**, 14, 4988.
2. Patera, L. L.; Queck, F.; Scheuerer, P.; Repp, J. Mapping orbital changes upon electron transfer with tunnelling microscopy on insulators. *Nature* **2019**, 566, 245-248.
3. Williams, J. O.; Jones, A. C.; Davies, M. J. Radiationless transitions in p-terphenyl crystals doped with anthracene, tetracene and pentacene. *J. Chem. Soc., Faraday Trans. 2*, **1983**, 79, 263-269.
4. Köhler, J.; Brouwer, A. C. J.; Groenen, E. J.; Schmidt, J. On the intersystem crossing of pentacene in p-terphenyl. *Chem. Phys. Lett.* **1996**, 250, 137-144.
5. Kasha, M. Characterization of electronic transitions in complex molecules. *Discuss Faraday Soc* **1950**, 9, 14-19.
6. Peng, J.; Sokolov, S.; Hernangómez-Pérez, D.; Evers, F.; Gross, L.; Lupton, J. M.; Repp, J. Atomically resolved single-molecule triplet quenching. *Science* **2021**, 373, 452-456.
7. Kong, F. F.; Tian, X.-J.; Zhang, Y.; Yu, Y. J.; Jing, S. H.; Zhang, Y.; Tian, G.-J.; Luo, Y.; Yang, J.-L.; Dong, Z.-C.; Hou, J. G. Probing intramolecular vibronic coupling through vibronic-state imaging. *Nat. Commun.* **2021**, 12, 1280.
8. Kimura, K.; Miwa, K.; Imada, H.; Imai-Imada, M.; Kawahara, S.; Takeya, J.; Kawai, M.; Galperin, M.; Kim, Y. Selective triplet exciton formation in a single molecule. *Nature* **2019**, 570, 210-213.
9. Pan, Y. Y.; Huang, J.; Wang, Z. M.; Yu, D. W.; Yang, B.; Ma, Y. G. Computational investigation on the large energy gap between the triplet excited-states in acenes. *RSC Adv.*, **2017**, 7, 26697-26703.
10. Coto, P. B.; Sharifzadeh, S.; Neaton, J. B.; Thoss, M. Low-lying electronic excited states of pentacene oligomers: A comparative electronic structure study in the context of singlet fission. *J. Chem. Theor. Comput.* **2015**, 11, 147-156.
11. Sangalli, D.; Romaniello, P.; Onida, G.; Marini, A. Double excitations in correlated systems: A many–body approach. *J. Chem. Phys.* **2011**, 134, 034115.
12. Repp, J.; Meyer, G.; Paavilainen, S.; Olsson, F. E.; Persson, M. Scanning tunneling spectroscopy of Cl vacancies in NaCl films: strong electron-phonon coupling in double-barrier tunneling junctions. *Phys. Rev. Lett.* **2005**, 95, 225503.
13. Fatayer, S.; Schuler, B.; Steurer, W.; Scivetti, I.; Repp, J.; Gross, L.; Persson, M.; Meyer, G. Reorganization energy upon charging a single molecule on an insulator measured by atomic force microscopy. *Nat. Nanotechnol.* **2018**, 13, 376-380.
14. Voigtländer, B. *Scanning probe microscopy: Atomic force microscopy and scanning tunneling microscopy* (Springer, 2015).
15. Fowler, R. H.; Nordheim, L. Electron emission in intense electric fields. *Proc. R. Soc. London. Ser. A*, **1928**, 119, 173-181.
16. Dweydari, A. W.; Mee, C. H. B. Oxygen adsorption on the (111) face of silver. *PSS A*, **1973**, *17*(1), 247-250.
17. Bennewitz, R.; Bammerlin, M.; Guggisberg, M.; Loppacher, C.; Baratoff, A.; Meyer, E.; Güntherodt, H. J. Aspects of dynamic force microscopy on NaCl/Cu(111): resolution, tip–

sample interactions and cantilever oscillation characteristics. *Surf. Interface Anal.* **1999**, 27, 462-466.
18. Ploigt, H. C.; Brun, C.; Pivetta, M.; Patthey, F.; Schneider, W. D. Local work function changes determined by field emission resonances: NaCl/Ag(100). *Phys. Rev. B* **2007**, 76, 195404.
19. Sellies, L.; Spachtholz, R.; Bleher, S.; Eckrich, J.; Scheuerer, P.; Repp, J. Single-molecule electron spin resonance by means of atomic force microscopy. *Nature* **2023**, 624, 64-68.
20. Gross, L.; Mohn, F.; Moll, N.; Liljeroth, P.; Meyer, G. The chemical structure of a molecule resolved by atomic force microscopy. *Science* **2009**, 325, 1110-1114.
21. Gross, L.; Schuler, B.; Mohn, F.; Moll, N.; Pavliček, N.; Steurer, W.; Scivetti, I.; Kotsis, K.; Persson, M.; Meyer, G. Investigating atomic contrast in atomic force microscopy and Kelvin probe force microscopy on ionic systems using functionalized tips, *Phys. Rev. B* **2014**, 90, 155455.
22. Wu, S. W.; Nazin, G. V.; Chen, X.; Qiu, X. H.; Ho, W. Control of relative tunneling rates in single molecule bipolar electron transport. *Phys. Rev. Lett.* **2004**, 93, 236802.
23. Zhang, L.; Yu, Y. J.; Chen, L. G.; Luo, Y.; Yang, B.; Kong, F. F.; Chen, G.; Zhang, Y.; Zhang, Q.; Luo, Y.; Yang, J. L., Dong, Z. C.; Hou, J. G. Electrically driven single-photon emission from an isolated single molecule. *Nat. Commun.* **2017**, 8, 580.
24. Hernangómez-Pérez, D.; Schlör, J.; Egger, D. A.; Patera, L. L.; Repp, J.; Evers, F. Reorganization energy and polaronic effects of pentacene on NaCl films. *Phys. Rev. B* **2020**, 102, 115419.
25. Friedrich, N.; Roslawska, A.; Arrieta, X.; Romeo, M.; Moal, E. L.; Scheurer, F.; Aizpurua, J.; Borisov, A. G.; Neuman, T.; Schull, G. Fluorescent single-molecule STM probe. *arXiv preprint* **2023**, *arXiv:2311.16805*.
26. Repp, J.; Meyer, G.; Stojković, S. M.; Gourdon, A.; Joachim, C. Molecules on insulating films: scanning-tunneling microscopy imaging of individual molecular orbitals. *Phys. Rev. Lett.* **2005**, 94, 026803.
27. Imai-Imada, M.; Imada, H.; Miwa, K.; Jung, J.; Shimizu, T. K.; Kawai, M.; Kim, Y. Energy-level alignment of a single molecule on ultrathin insulating film. *Phys. Rev. B* **2018**, 98, 201403.
28. Scivetti, I.; Persson, M. Frontier molecular orbitals of a single molecule adsorbed on thin insulating films supported by a metal substrate: electron and hole attachment energies. *J. Condens. Matter Phys.* **2017**, 29, 355002.
29. Cochrane, K. A.; Schiffrin, A.; Roussy, T. S.; Capsoni, M.; Burke, S. A. Pronounced polarization-induced energy level shifts at boundaries of organic semiconductor nanostructures. *Nat. Commun.* **2015**, 6, 8312.
30. Faber, C.; Boulanger, P.; Attaccalite, C.; Duchemin, I.; Blase, X. Excited states properties of organic molecules: from density functional theory to the *GW* and Bethe–Salpeter Green's function formalisms, *Phil. Trans. R. Soc. A* **2014**, 372, 20130271.
31. Esat, T.; Friedrich, N.; Tautz, F.S.; and Temirov, R. A standing molecule as a single-electron field emitter. *Nature* **2018**, 558, 573.
32. Chiesa, A.; Carretta, S.; Santini, P.; Amoretti, G.; Pavarini, E. Many-Body Models for Molecular Nanomagnets. *Phys. Rev. Lett.* **2013**, 110, 157204.
33. Hettler, M.H.; Wenzel, W.; Wegewijs, M.R.; Schoeller, H.; Current Collapse in Tunneling Transport through Benzene. *Phys. Rev. Lett.* **2003**, 90, 076805.

34. Yu, P.; Kocić, N.; Repp, J.; Siegert, B.; Donarini, A. Apparent Reversal of Molecular Orbitals Reveals Entanglement. *Phys. Rev. Lett.* **2017**, 119, 056801.
35. Miwa, K.; Imada, H.; Imai-Imada, M.; Kimura, K.; Galperin, M.; Kim Y. Many-Body State Description of Single-Molecule Electroluminescence Driven by a Scanning Tunneling Microscope. *Nano Letters* **2019**, 19, 2803.